

Transfer Learning of Surrogate Models: Integrating Domain Warping and Affine Transformations

Shuaiqun Pan
LIACS, Leiden University
Leiden, The Netherlands
s.pan@liacs.leidenuniv.nl

Diederick Vermetten
LIACS, Leiden University
Leiden, The Netherlands
d.l.vermetten@liacs.leidenuniv.nl

Manuel López-Ibáñez
University of Manchester
Manchester, UK
manuel.lopez-
ibanez@manchester.ac.uk

Thomas Bäck
LIACS, Leiden University
Leiden, The Netherlands
t.h.w.baeck@liacs.leidenuniv.nl

Hao Wang
LIACS, Leiden University
Leiden, The Netherlands
h.wang@liacs.leidenuniv.nl

ABSTRACT

Surrogate models provide efficient alternatives to computationally demanding real-world processes but often require large datasets for effective training. A promising solution to this limitation is the transfer of pre-trained surrogate models to new tasks. Previous studies have investigated the transfer of differentiable and non-differentiable surrogate models, typically assuming an affine transformation between the source and target functions. This paper extends previous research by addressing a broader range of transformations, including linear and nonlinear variations. Specifically, we consider the combination of an unknown input warping—such as one modeled by the beta cumulative distribution function—with an unspecified affine transformation. Our approach achieves transfer learning by employing a limited number of data points from the target task to optimize these transformations, minimizing empirical loss on the transfer dataset. We validate the proposed method on the widely used Black-Box Optimization Benchmark (BBOB) testbed and a real-world transfer learning task from the automobile industry. The results underscore the significant advantages of the approach, revealing that the transferred surrogate significantly outperforms both the original surrogate and the one built from scratch using the transfer dataset, particularly in data-scarce scenarios.

CCS CONCEPTS

• **Computing methodologies** → **Transfer learning**; • **Theory of computation** → *Gaussian processes*; Continuous optimization.

KEYWORDS

transfer learning, Gaussian process, input warping, affine transformation, Riemannian gradient

ACM Reference Format:

Shuaiqun Pan, Diederick Vermetten, Manuel López-Ibáñez, Thomas Bäck, and Hao Wang. 2025. Transfer Learning of Surrogate Models: Integrating Domain Warping and Affine Transformations. In *Genetic and Evolutionary Computation Conference (GECCO '25)*, July 14–18, 2025, Malaga, Spain. ACM, New York, NY, USA, 19 pages. <https://doi.org/XXXXXXXX.XXXXXXX>

1 INTRODUCTION

Surrogate modeling [3, 15, 16, 41] is extensively used to replace expensive simulators for reducing computational costs, for instance in automobile industry [13, 22, 30, 39]. Machine learning models are commonly used as surrogates, e.g., Gaussian process regression (GPR) [29, 31, 34] and random forest [1, 43]. Training a surrogate model on a new problem often requires a large number of training samples, in particular when there are many independent variables. Acquiring this data usually implies running expensive simulations or real-world experiments. Therefore, we wish to avoid the cost of acquiring large data sets to build surrogates on a new problem instance. Transfer learning [26, 45, 49] can be used to tackle this issue: with a tiny transfer data set sampled on a new problem (the target), we can learn to tweak an accurate surrogate trained on an old problem (the source), provided certain symmetry/invariances between problems.

Covariance shift [28, 35, 38] is an important type of symmetry, which says that for a regression task to approximate the source function $f^S: \mathbb{R}^d \rightarrow \mathbb{R}$, a target function f^T can be obtained from f^S by transforming the domain thereof. Namely, there exists a bijection $g: \mathbb{R}^d \rightarrow \mathbb{R}^d$ such that $f^T = f^S \circ g$. As for the surrogate modeling, the covariance shift implies the predictive distribution $P(y|x)$ remains unchanged between the source and the target while $P(x)$ differs. Previous studies [24, 25] have investigated a special case: g being an affine transformation, where the transformation is learned by minimizing a loss function on a tiny transfer data evaluated on the target.

However, the affine transformation g might be too restrictive to model complex real-world scenarios, e.g., non-linearity is necessary in the automobile industry problems [25]. Hence, we propose implementing a non-linear g function with a beta cumulative distribution function (CDF) [37]. We showcase the preliminary results of our method in Figure 1, where we train a Gaussian process regression (GPR) model train on function F7 from the BBOB benchmark suite.

Permission to make digital or hard copies of all or part of this work for personal or classroom use is granted without fee provided that copies are not made or distributed for profit or commercial advantage and that copies bear this notice and the full citation on the first page. Copyrights for components of this work owned by others than the author(s) must be honored. Abstracting with credit is permitted. To copy otherwise, or republish, to post on servers or to redistribute to lists, requires prior specific permission and/or a fee. Request permissions from permissions@acm.org.

GECCO '25, July 14–18, 2025, Malaga, Spain

© 2025 Copyright held by the owner/author(s). Publication rights licensed to ACM.

ACM ISBN 978-1-4503-XXXX-X/18/06...\$15.00

<https://doi.org/XXXXXXXX.XXXXXXX>

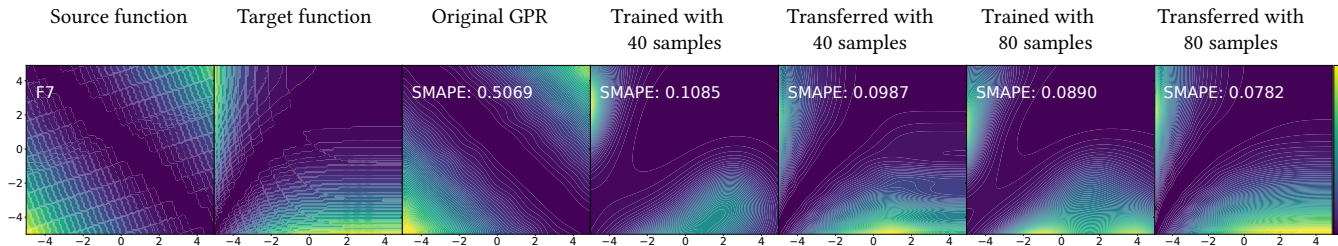


Figure 1: On the two-dimensional F7 StepEllipsoid function, we show, from left to right, the contour lines of the source function (f^S), the target (f^T), the original GPR (\hat{f}^S) trained to approximate f^S , the GPR model trained from scratch with 40 points sampled on f^T , and the original GPR model transferred with these 40 points. f^T is created from f^S by transforming the domain thereof with affine warping. We show the transfer effect with 80 data points in the last two subplots.

Comparing the transferred model to the one trained from scratch on the target function (fourth and fifth subplots), we see the transferred model is more accurate and resembles the contour lines of the target function. Our contributions are:

- We introduce the non-linear input warping (beta CDF) to affine transfer learning proposed in [24], realizing a novel non-linear domain transfer method.
- We numerically validate the effectiveness of our approach on synthetic transfer learning problems created from the Black-Box Optimization Benchmark (BBOB) suite and on a real-world application in the automobile industry.
- We analyze the benchmarking outcomes to identify the conditions under which the transferred model outperforms the one trained from scratch.

The paper is organized as follows: Sec. 2 briefly reviews the related works. In Sec. 3, we describe our methodology, followed by details of the experimental setup and synthetic and real-world transfer learning problems (Sec. 4). In Sec. 5, we provide a comprehensive analysis and discussion of the experimental results. Sec. 6 summarizes the key empirical findings and points out the next steps.

2 RELATED WORKS

Transfer learning for GPR. Saida and Nishio [33] investigated GPR surrogate model transfer for structural reliability under uncertainties by augmenting the feature space [9]. Zhang et al. [47] proposed a novel transfer learning strategy that employs a geodesic flow kernel and knee point-based manifold learning to refine Gaussian process models using high-quality knee solutions from previous tasks, thereby enriching training data and boosting solution precision. In multi-task learning, Cao et al. [5] developed the Adaptive Transfer Learning algorithm (AT-GP) using a semi-parametric transfer kernel. The Transfer Bayesian Committee Machine (Tr-BCM) [8] introduced a scalable transfer learning approach by aggregating predictions from lightweight local experts, relaxing assumptions of uniform similarity between tasks. Recent advances include Papez and Quinn [27], which proposed a probabilistic predictor for global source-target interactions, and Wei et al. [44], which developed an interpretable multi-source transfer kernel for improved cross-task performance.

Transfer learning with input warping. Snoek et al. [37] propose warping the independent variables with beta CDF to realize non-stationary kernels, where the unknown shape parameters of the beta distribution are inferred with Bayesian estimation (using log-normal priors). Their posterior predictive distribution is obtained by marginalizing the shape parameters. In contrast, in this work, we use the beta CDF to model the non-linear relation between the domain of the source and the target function. Also, we learn the unknown shape parameters with a loss-minimization approach. Cowen-Rivers et al. [7] introduced Kumaraswamy input warping, offering a more computationally efficient alternative to the beta CDF with similar flexibility. Du et al. [11] presented a Hypothesis Transfer Learning framework linking domains via transformation functions, and Zhu et al. [48] proposed a nonlinear transformation method to align the marginal probability distributions without prior data knowledge.

3 LEARNING AFFINE WARPING TO TRANSFER DOMAINS

Context. We consider a source regression task: a source function $f^S: \mathbb{R}^d \rightarrow \mathbb{R}$ to generate the regression data and a trained surrogate model \hat{f}^S that approximates f^S accurately. Consider a new regression task f^T , the target task. We assume that there exists an unknown nonlinear symmetry between f^S and $f^T: \forall \mathbf{x} \in \mathbb{R}^d, f^T(\mathbf{x}) = f^S \circ g(\mathbf{x}), g(\mathbf{x}) = \mathbf{W}\phi(\mathbf{x}) + \mathbf{v}$, where $\mathbf{v} \in \mathbb{R}^d, \mathbf{W} \in \text{SO}(d)$ (the rotation group of dimension d), and $\phi: \mathbb{R}^d \rightarrow \mathbb{R}^d$ is a non-linear diffeomorphism.

Goal. We wish to transfer the source surrogate model \hat{f}^S to the target function f^T by re-parameterizing it as $\hat{f}^S(\mathbf{W}\phi(\mathbf{x}) + \mathbf{v})$ and learn the unknown parameters \mathbf{W}, \mathbf{v} , and ϕ with a small transfer data set $\mathcal{T} = \{(\mathbf{x}^k, f^T(\mathbf{x}^k))\}_{k=1}^{n_T}$ from the target function.

Method. For the non-linear function ϕ , we consider representing it with the beta cumulative distribution function (CDF) [37]:

$$\phi(\mathbf{x}; \theta) = (\phi_1(x_1, \alpha_1, \beta_1), \dots, \phi_i(x_i, \alpha_i, \beta_i), \dots, \phi_d(x_d, \alpha_d, \beta_d)) \quad (1)$$

$$\phi_i(x_i, \alpha_i, \beta_i) = \int_0^{x_i} \frac{u^{\alpha_i-1}(1-u)^{\beta_i-1}}{B(\alpha_i, \beta_i)} du \quad (2)$$

$$\theta = (\alpha_1, \beta_1, \dots, \alpha_i, \beta_i, \dots, \alpha_d, \beta_d) \in \mathbb{R}_{>0}^{2d} \quad (3)$$

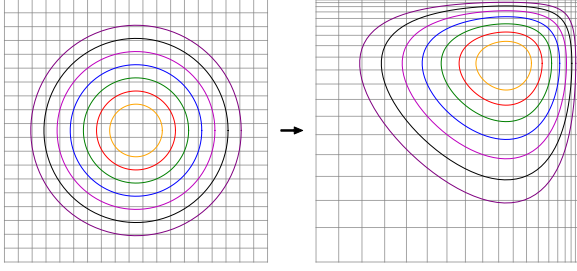


Figure 2: 2D input warping. The coordinate system is transformed from left to right by beta CDFs with shape parameter $\alpha = 1.0558, \beta = 1.9339$ for x -axis and $\alpha = 0.8655, \beta = 1.8148$ for y -axis. We show the contour lines of a sphere function on the left and its warped version on the right.

where $B(\alpha_i, \beta_i)$ is the beta function. The beta CDF parameterization for each dimension has two unknown parameters $\alpha_i > 0, \beta_i > 0$. We illustrate the effect of input warping for a 2D sphere function in Fig. 2, where each axis is warping non-linearly with different shape parameters.

REMARK. (1) The beta CDF preserves the convexity of the surrogate since it is a smooth, monotonic transformation. (2) For non-universal models, e.g., GPR with a fixed kernel, the beta CDF materializes a non-stationary auto-correlation function, increasing such models' expressivity. (3) For universal models, e.g., deep neural networks, the beta CDF can reshape the input space and make some target functions easier to learn, which is similar to the effect of the normalizing flow [32].

On the transfer data set \mathcal{T} , we measure the mean squared error of the re-parameterized source model:

$$\mathcal{L}: \mathbb{R}^d \times \text{SO}(d) \times \mathbb{R}_{>0}^{2d} \rightarrow \mathbb{R}, \quad (4)$$

$$(\mathbf{v}, \mathbf{W}, \theta) \mapsto \frac{1}{n_{\mathcal{T}}} \sum_{\mathbf{x} \in \mathcal{T}} \left(\hat{f}^S(\mathbf{W}(\phi(\mathbf{x}; \theta)) + \mathbf{v}) - f^T(\mathbf{x}) \right)^2.$$

We solve the transfer learning task by minimizing the above MSE loss. We shall discuss tackling this minimization problem for differentiable and non-differentiable surrogate models.

3.1 Transfer differentiable surrogates

If the surrogate model is continuously differentiable, e.g., Gaussian process regression or support vector machine, we can minimize Eq. (4) with mini-batch gradient descent. Let $\mathbf{y}^k = \mathbf{W}\phi(\mathbf{x}^k; \theta)$ and

y_i^k be i -th component of \mathbf{y}^k . The gradient of \mathcal{L} is:

$$\frac{\partial \mathcal{L}}{\partial v_i} = \frac{2}{n_{\mathcal{T}}} \sum_{k=1}^{n_{\mathcal{T}}} \left(\hat{f}^S(\mathbf{y}^k) - f^T(\mathbf{x}^k) \right) \frac{\partial \hat{f}^S}{\partial y_i^k} \quad (5)$$

$$\frac{\partial \mathcal{L}}{\partial W_{ij}} = \frac{2}{n_{\mathcal{T}}} \sum_{k=1}^{n_{\mathcal{T}}} \left(\hat{f}^S(\mathbf{y}^k) - f^T(\mathbf{x}^k) \right) \phi_j(x_j^k, \alpha_j, \beta_j) \frac{\partial \hat{f}^S}{\partial y_i^k} \quad (6)$$

$$\frac{\partial \mathcal{L}}{\partial \alpha_i} = \frac{2}{n_{\mathcal{T}}} \sum_{k=1}^{n_{\mathcal{T}}} \sum_{\ell=1}^d \left(\hat{f}^S(\mathbf{y}^k) - f^T(\mathbf{x}^k) \right) \frac{\partial \hat{f}^S}{\partial y_{\ell}^k} W_{\ell i} \frac{\partial \phi_i(x_i^k, \alpha_i, \beta_i)}{\partial \alpha_i} \quad (7)$$

$$\frac{\partial \mathcal{L}}{\partial \beta_i} = \frac{2}{n_{\mathcal{T}}} \sum_{k=1}^{n_{\mathcal{T}}} \sum_{\ell=1}^d \left(\hat{f}^S(\mathbf{y}^k) - f^T(\mathbf{x}^k) \right) \frac{\partial \hat{f}^S}{\partial y_{\ell}^k} W_{\ell i} \frac{\partial \phi_i(x_i^k, \alpha_i, \beta_i)}{\partial \beta_i} \quad (8)$$

The derivatives ϕ_i w.r.t. α_i and β_i are

$$\frac{\partial \phi(x_i, \alpha_i, \beta_i)}{\partial \alpha_i} = A(x_i, \alpha_i, \beta_i) - \phi(x_i; \alpha_i, \beta_i) \frac{\partial}{\partial \alpha_i} \log B(\alpha_i, \beta_i) \quad (9)$$

$$\frac{\partial \phi(x_i, \alpha_i, \beta_i)}{\partial \beta_i} = B(x_i, \alpha_i, \beta_i) - \phi(x_i; \alpha_i, \beta_i) \frac{\partial}{\partial \beta_i} \log B(\alpha_i, \beta_i) \quad (10)$$

$$A(x_i, \alpha_i, \beta_i) = \int_0^{x_i} \frac{\log(u) u^{\alpha_i-1} (1-u)^{\beta_i-1}}{B(\alpha_i, \beta_i)} du \quad (11)$$

$$B(x_i, \alpha_i, \beta_i) = \int_0^{x_i} \frac{\log(1-u) u^{\alpha_i-1} (1-u)^{\beta_i-1}}{B(\alpha_i, \beta_i)} du \quad (12)$$

$$\frac{\partial \log B(\alpha_i, \beta_i)}{\partial \alpha_i} = \psi(\alpha_i) - \psi(\alpha_i + \beta_i) \quad (13)$$

$$\frac{\partial \log B(\alpha_i, \beta_i)}{\partial \beta_i} = \psi(\beta_i) - \psi(\alpha_i + \beta_i) \quad (14)$$

where ψ is the digamma function and $\partial \hat{f}^S / \partial y_i^k$ can be computed analytically from surrogate's predictor. All the above derivatives live in Euclidean spaces, to which the vanilla gradient descent algorithm can be applied. However, $\mathbf{W} \in \text{SO}(d)$ is a rotation matrix, and it will not remain in $\text{SO}(d)$ if we perform a descent step with Euclidean gradient $\partial \mathcal{L} / \partial W_{ij}$. Hence, we decide to take a Riemannian gradient descent method, which first computes the Riemannian gradient - an orthogonal projection of $\partial \mathcal{L} / \partial W_{ij}$ onto the tangent space of $\text{SO}(d)$ at \mathbf{W} [24]:

$$\nabla_{\mathbf{R}} \mathcal{L}(\mathbf{W}) = \mathbf{P} \left(\frac{\partial \mathcal{L}}{\partial \mathbf{W}} \right), \quad \mathbf{P}(\mathbf{M}) = \mathbf{W} \frac{\mathbf{W}^T \mathbf{M} - \mathbf{M}^T \mathbf{W}}{2}, \quad (15)$$

Next, a gradient step (geodesic with initial velocity $\nabla_{\mathbf{R}} \mathcal{L}(\mathbf{W})$) on $\text{SO}(d)$ from \mathbf{W} can be computed by the exponential map:

$$\text{Exp}_{\mathbf{W}}(\sigma \nabla_{\mathbf{R}} \mathcal{L}(\mathbf{W})) = \mathbf{W} \text{Exp}(\sigma \mathbf{W}^T \nabla_{\mathbf{R}} \mathcal{L}(\mathbf{W})) \in \text{SO}(d), \quad (16)$$

where σ is the step-size and Exp is the matrix exponential.

3.2 Transfer non-differentiable surrogates

We also wish to apply our methodology to non-differentiable models like random forests. We propose to use the Covariance matrix adaptation evolution strategy (CMA-ES) [12, 17, 18] to tune the parameters. CMA-ES can be applied directly to the search space of the translation parameter \mathbf{v} and the beta CDF parameters α and β , which are Euclidean. However, special treatment is needed for \mathbf{W} , which lives in a smooth manifold $\text{SO}(d)$. To solve this issue, we consider the Lie group representation $\mathfrak{so}(d) = \{\mathbf{A} \in \mathbb{R}^{d \times d} : \mathbf{A}^T = -\mathbf{A}\}$, which is a flat space (with dimension $d(d-1)/2$), and optimize

this representation with CMA-ES. A rotation matrix \mathbf{W} can be recovered from its representation \mathbf{A} with the exponential map, i.e., $\mathbf{W} = \text{Exp}(\mathbf{A})$. For each search point $\mathbf{z} \in \mathbb{R}^{d(d-1)/2}$, we have to transform it into a $d \times d$ antisymmetric matrix to preserve the structure of $\mathfrak{so}(d)$: the components in \mathbf{z} are sequentially assigned to the upper triangular of \mathbf{A} (diagonal entries are zero) row by row. The negative value of the transposition of the upper triangular then fills the lower triangular entries.

4 EXPERIMENTAL SETTINGS

Synthetic tasks based on BBOB. We first evaluate our method on the Black-Box Optimization Benchmarking (BBOB) [19–21] suite, which consists of 24 continuous, single-objective problems. The BBOB suite has been widely used as a regression benchmark [6, 36, 40, 46] as it reflects real-world regression difficulties. To create synthetic transfer learning problems out of BBOB, we take the first problem instance of each BBOB function as the source f^S , and construct the target f^T by applying a beta CDF transformation, followed by random rotation and translation transformations, to the base function. The shape parameters are sampled from log-normal distributions, i.e., $\log \alpha_i \sim \mathcal{N}(\mu_i^\alpha, \sigma_i^\alpha)$, $\log \beta_i \sim \mathcal{N}(\mu_i^\beta, \sigma_i^\beta)$. Inspired by [37], we choose different priors to realize distinct shapes of the beta CDF:

- linear shape: $\mu_i^\alpha = \mu_i^\beta = 0$, $\sigma_i^\alpha = \sigma_i^\beta = 0.5$
- exponential shape: $\mu_i^\alpha = 0$, $\sigma_i^\alpha = 0.25$, $\mu_i^\beta = 1$, $\sigma_i^\beta = 1$
- logarithmic shape: $\mu_i^\alpha = 1$, $\sigma_i^\alpha = 1$, $\mu_i^\beta = 0$, $\sigma_i^\beta = 0.25$
- Sigmoidal shape: $\mu_i^\alpha = \mu_i^\beta = 2$, $\sigma_i^\alpha = \sigma_i^\beta = 0.5$

To generate the training data set for f^S , we sample $1000 \times d$ points uniformly at random in the domain $[-5, 5]^d$ and evaluate them on f^S . To assess the performance of the original GPR model \hat{f}^S on the target function f^T , we create an independent test dataset of the same size, $1000 \times d$, sampled uniformly at random from f^T . The transfer learning process uses a transfer dataset \mathcal{T} , containing $40 \times d$ randomly sampled points from f^T . In addition, we consider a minimal transfer dataset of 40 points, independent of the dimensionality of the target problem, smaller datasets of 20 points for 2-dimensional and 5-dimensional cases, and a larger dataset of 80 points for the 10-dimensional problems. After transfer learning, the effectiveness of the transferred GPR model \hat{f}^T is evaluated using the same test set employed for the original GPR model. We also train a GPR model from scratch directly on \mathcal{T} for comparison.

Real-world benchmark from automobile industry. This dataset evaluates the performance of optimization algorithms in the context of automotive engineering, with a specific focus on minimizing braking distances. It includes five distinct vehicle configurations, each characterized by unique combinations of tire performance and vehicle load conditions. The search space consists of two Anti-lock Braking System (ABS) control parameters, x_1 and x_2 , which span a total of 10 101 discrete parameter combinations [39].

We construct the surrogate model \hat{f}^S for the source functions to validate our proposed transfer learning approach on this dataset by utilizing the entire f^S dataset. The complete dataset is also employed as the test set to compute the SMAPE for different GPR

models on the target function f^T . The transfer dataset \mathcal{T} is randomly sampled from the target function, with a maximum of up to 50 points. A GPR model is also trained from scratch using only the same transfer dataset without incorporating any prior knowledge. Additionally, we analyze how varying the size of \mathcal{T} , ranging from 5 to 50 points, impacts the performance of the transfer learning approach. Additionally, we include a reproduced baseline method that focuses exclusively on transfer learning using affine transformations only for this dataset [24].

Performance measure. We measure the models' performance using the symmetric mean absolute percentage error (SMAPE) [14]. To ensure robustness and reliability, the transfer learning process is conducted ten times for each BBOB function, using randomly generated beta CDF and affine transformation in each iteration. Likewise, the real-world application in the automotive industry is repeated ten times to account for variability.

Implementation details. The BBOB functions are accessed via the IOHexperimenter framework [10]. We implement a GPR model with a Gaussian kernel with the GPy package.¹ To mitigate the skewness of the function values, a *log*-transformation is applied thereto before training the surrogate model for both synthetic and real-world problems. We use an exponentially decaying learning rate scheduler for the mini-batch gradient descent to minimize the loss function. Hyperparameter tuning for the transfer learning procedure included adjusting the learning rate ($[10^{-3}, 1]$), batch size ($[\lceil 0.1|\mathcal{T}|, 0.2|\mathcal{T}|]$), number of epochs ($[60, 100]$), and the decay rate of the exponential scheduler ($[5 \times 10^{-3}, 0.3]$). These hyperparameters are independently fine-tuned for each BBOB function using the SMAC3 library [23]. The experimental setup details and implementations are available via Zenodo [2]. Additionally, a copy of the supplementary materials is also included.

5 EXPERIMENTAL RESULTS

5.1 Transferring GPR on BBOB

In Fig. 3, we compare the transferred GPR to the one trained from scratch on each 2-dimensional BBOB function regarding the average SMAPE difference. This analysis investigates the effectiveness of transfer learning with different transfer sample sizes and beta CDF parameterizations. The results reveal that, with only 20 transfer samples, the transferred model performs better for most of the function and beta parameterization combinations. However, as the number of transfer samples increases, the performance advantage decreases until it becomes negative for a sample size of 80. Also, the transfer learning method fails to improve on F24, which has a highly rugged landscape.

Additional analyses in Fig. 8 and Fig. 9 (refer to the supplementary material [2]) extend these observations to 5D and 10D BBOB functions. In the 5D case, models trained from scratch demonstrate a more noticeable advantage compared to the 2D scenario, surpassing transferred models on certain BBOB functions with as few as 20 samples. This could be because the 5D case involves more complex relations, which the transferred models find harder to capture than the simpler or more closely related 2D case. Interestingly, in the 10D experiments, models trained from scratch exhibit significant

¹<https://gpy.readthedocs.io/en/deploy/>

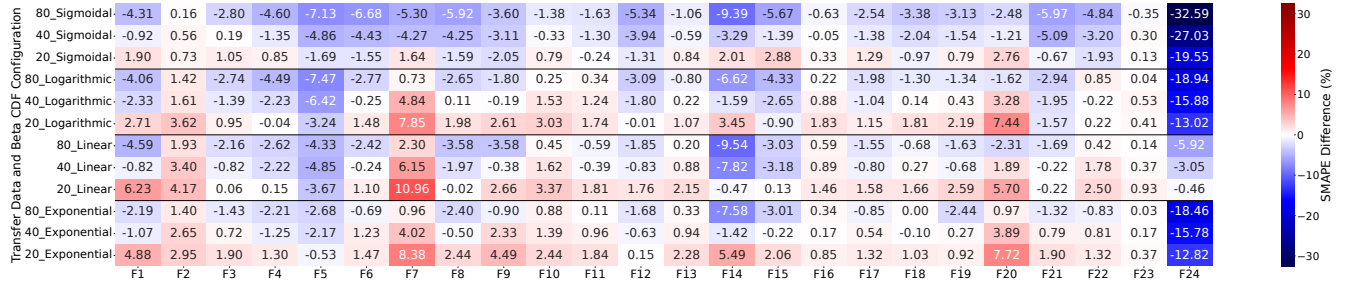


Figure 3: On 2D BBOB functions, we compare the transferred GPR models with those trained from scratch on the transfer dataset. Each cell displays the percentage difference in average SMAPE (%) for a combination of BBOB functions, sample size, and beta CDF shape. Positive values (shown in red) indicate superior performance of the transferred model and vice versa.

2D	Original GPR	Train from scratch		Transferred		Train from scratch		Transferred	
		20 samples		40 samples		80 samples			
F1	0.3701 ± 0.0370	0.1080 ± 0.0467	<u>0.0592 ± 0.0397</u>	0.0580 ± 0.0212	<u>0.0687 ± 0.0240</u>	0.0390 ± 0.0159	<u>0.0609 ± 0.0429</u>		
F2	0.1365 ± 0.0195	0.0613 ± 0.0219	<u>0.0318 ± 0.0183</u>	0.0561 ± 0.0190	<u>0.0296 ± 0.0178</u>	0.0442 ± 0.0156	<u>0.0302 ± 0.0182</u>		
F3	0.2686 ± 0.0504	0.0754 ± 0.0308	<u>0.0564 ± 0.0240</u>	0.0584 ± 0.0202	<u>0.0512 ± 0.0158</u>	0.0345 ± 0.0106	<u>0.0488 ± 0.0195</u>		
F4	0.2676 ± 0.0561	0.0675 ± 0.0255	<u>0.0545 ± 0.0116</u>	0.0477 ± 0.0132	<u>0.0602 ± 0.0289</u>	0.0312 ± 0.0087	<u>0.0533 ± 0.0217</u>		
F5	0.2653 ± 0.0709	0.0419 ± 0.0188	<u>0.0472 ± 0.0283</u>	0.0244 ± 0.0127	<u>0.0461 ± 0.0277</u>	0.0153 ± 0.0122	<u>0.0421 ± 0.0268</u>		
F6	0.3651 ± 0.1498	0.0865 ± 0.1002	<u>0.0718 ± 0.0625</u>	0.0751 ± 0.0784	<u>0.0628 ± 0.0483</u>	0.0557 ± 0.0473	<u>0.0626 ± 0.0500</u>		
F7	0.4115 ± 0.0824	0.1615 ± 0.0626	<u>0.0777 ± 0.0357</u>	0.1151 ± 0.0406	<u>0.0749 ± 0.0379</u>	0.0851 ± 0.0249	<u>0.0755 ± 0.0327</u>		
F8	0.3414 ± 0.0552	0.1378 ± 0.0551	<u>0.1134 ± 0.0544</u>	0.1015 ± 0.0573	<u>0.1065 ± 0.0442</u>	0.0709 ± 0.0409	<u>0.0949 ± 0.0446</u>		
F9	0.3564 ± 0.0595	0.1276 ± 0.0716	<u>0.0827 ± 0.0443</u>	0.1102 ± 0.0706	<u>0.0869 ± 0.0436</u>	0.0714 ± 0.0363	<u>0.0804 ± 0.0347</u>		
F10	0.1477 ± 0.0315	0.0677 ± 0.0261	<u>0.0433 ± 0.0228</u>	0.0586 ± 0.0177	<u>0.0447 ± 0.0226</u>	0.0493 ± 0.0136	<u>0.0405 ± 0.0227</u>		
F11	0.1913 ± 0.0793	0.0697 ± 0.0305	<u>0.0513 ± 0.0265</u>	0.0564 ± 0.0235	<u>0.0468 ± 0.0281</u>	0.0469 ± 0.0138	<u>0.0458 ± 0.0268</u>		
F12	0.3242 ± 0.0535	0.0527 ± 0.0239	<u>0.0512 ± 0.0232</u>	0.0418 ± 0.0156	<u>0.0481 ± 0.0258</u>	0.0318 ± 0.0151	<u>0.0486 ± 0.0252</u>		
F13	0.1815 ± 0.0210	0.0601 ± 0.0198	<u>0.0373 ± 0.0151</u>	0.0492 ± 0.0105	<u>0.0398 ± 0.0223</u>	0.0400 ± 0.0080	<u>0.0367 ± 0.0189</u>		
F14	0.5601 ± 0.0838	0.1666 ± 0.0710	<u>0.1117 ± 0.0678</u>	0.1112 ± 0.0363	<u>0.1254 ± 0.0609</u>	0.0554 ± 0.0194	<u>0.1312 ± 0.0672</u>		
F15	0.3755 ± 0.1195	0.0833 ± 0.0351	<u>0.0627 ± 0.0330</u>	0.0536 ± 0.0171	<u>0.0558 ± 0.0228</u>	0.0362 ± 0.0159	<u>0.0663 ± 0.0329</u>		
F16	0.2039 ± 0.0268	0.1433 ± 0.0353	<u>0.1348 ± 0.0304</u>	0.1334 ± 0.0270	<u>0.1317 ± 0.0227</u>	0.1246 ± 0.0256	<u>0.1212 ± 0.0252</u>		
F17	0.5333 ± 0.1150	0.1368 ± 0.0389	<u>0.1236 ± 0.0340</u>	0.1215 ± 0.0363	<u>0.1161 ± 0.0291</u>	0.1076 ± 0.0300	<u>0.1161 ± 0.0294</u>		
F18	0.4151 ± 0.0884	0.1047 ± 0.0372	<u>0.0944 ± 0.0263</u>	0.0926 ± 0.0304	<u>0.0936 ± 0.0277</u>	0.0848 ± 0.0272	<u>0.0848 ± 0.0229</u>		
F19	0.4308 ± 0.1200	0.1499 ± 0.0447	<u>0.1407 ± 0.0486</u>	0.1339 ± 0.0386	<u>0.1312 ± 0.0442</u>	0.1111 ± 0.0343	<u>0.1355 ± 0.0415</u>		
F20	0.4005 ± 0.0336	0.1500 ± 0.0820	<u>0.0728 ± 0.0616</u>	0.1097 ± 0.0588	<u>0.0708 ± 0.0556</u>	0.0788 ± 0.0380	<u>0.0691 ± 0.0505</u>		
F21	0.3857 ± 0.0605	0.1972 ± 0.0439	<u>0.1782 ± 0.0491</u>	0.1807 ± 0.0411	<u>0.1728 ± 0.0401</u>	0.1693 ± 0.0383	<u>0.1825 ± 0.0428</u>		
F22	0.2972 ± 0.0390	0.1577 ± 0.0370	<u>0.1445 ± 0.0405</u>	0.1463 ± 0.0376	<u>0.1382 ± 0.0378</u>	0.1312 ± 0.0294	<u>0.1395 ± 0.0358</u>		
F23	0.1543 ± 0.0122	0.1575 ± 0.0185	<u>0.1538 ± 0.0124</u>	0.1556 ± 0.0168	<u>0.1539 ± 0.0127</u>	0.1541 ± 0.0149	<u>0.1538 ± 0.0128</u>		
F24	0.4134 ± 0.2179	0.1821 ± 0.0660	0.3103 ± 0.1820	0.1503 ± 0.0434	0.3081 ± 0.1839	0.1214 ± 0.0365	0.3060 ± 0.1857		

Table 1: On 2D BBOB functions, we compare the SMAPE value (mean ± standard deviation) of three GPR models: the original model, the transferred model, and the one trained from scratch on the transfer dataset. Three transfer sample sizes are investigated $|\mathcal{T}| \in \{20, 40, 80\}$. The transfer target is created with an exponential-shaped beta CDF. We apply the Kruskal-Wallis test with a significance level of 5%, followed by Dunn’s post-hoc analysis to detect significant winners: the transferred model is underlined if it outperforms the original model; the boldface indicates the better one between the transferred and the model trained from scratch.

performance drops with only 40 samples. A similar issue is observed for some BBOB functions even with 80 samples, as such sample sizes are insufficient to train accurate GPR models [4, 42]. These results align with prior studies [24], which emphasize the value of transfer learning in data-scarce settings but highlight its diminishing returns as data availability grows.

Next, we show the detailed performance values of the 2D scenario in Table 1. Results for 5D and 10D cases are in the supplementary material [2]. To assess the impact of transfer sample size, we compare models using the Kruskal-Wallis test and Dunn’s post-hoc analysis (5% significance). Significant results are highlighted: the transferred model is underlined when it outperforms the original,

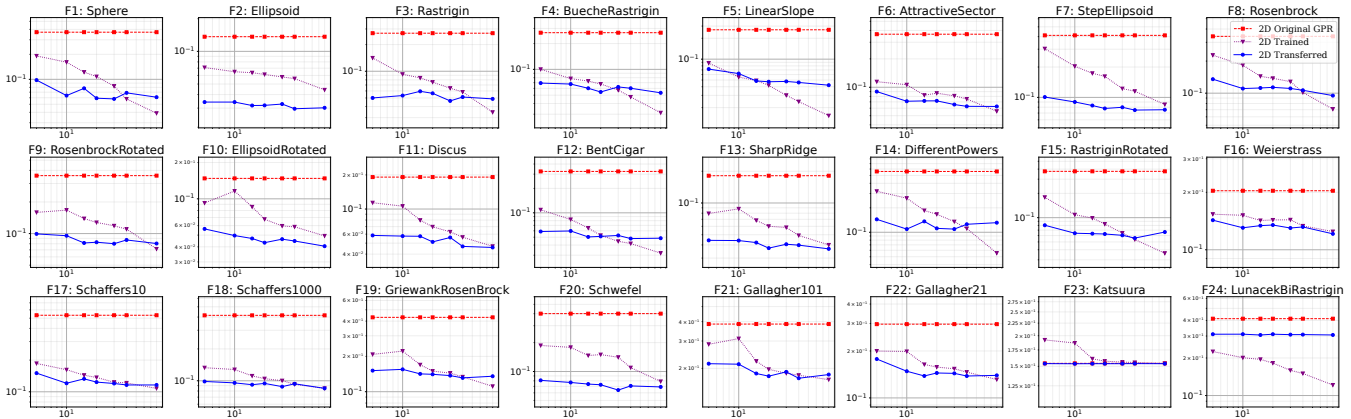


Figure 4: The SMAPE values (y -axis) for the original GPR, transferred GPR, and GPR trained solely on the transfer dataset are plotted against the transfer dataset sizes (x -axis: 5, 10, 15, 20, 30, 40, 80) for 2D BBOB functions. The analysis combines a beta CDF warping function (approximating an exponential transformation) with an affine transformation.

and the better model between transferred and trained-from-scratch is highlighted in boldface when statistically significant.

For 2D functions, the transferred GPR generally outperforms the model trained from scratch and the original GPR when only 20 transfer samples are available, with F5 and F24 being notable exceptions. However, as the transfer sample size increases to 80, most functions perform better with the model trained from scratch than the transferred model. Despite this, the transferred model consistently delivers significant improvements over the original GPR across all transfer sample sizes, except for F23 and F24. Fig. 4 further explores the relation between model performance and transfer sample sizes. The SMAPE trends show that the transferred model consistently outperforms the model trained from scratch up to 40 sample points for most functions, after which the advantage gradually diminishes. This demonstrates the effectiveness of our transfer learning approach in low-data scenarios, as anticipated. Interestingly, for F5, there is a relatively simple linear function—the model trained from scratch surpasses the transferred model with as few as 20 samples, likely due to the low sample complexity of F5, enabling accurate predictions with minimal data. A detailed analysis reveals that the original GPR model for F23 and F24 suffers from significant underfitting, particularly in the case of F23, which limits the potential benefits of transfer learning. This finding emphasizes that the effectiveness of the transfer learning approach depends on the original GPR model achieving a baseline level of accuracy. Furthermore, the SMAPE trends for F24 highlight specific limitations of the proposed method, indicating that while effective overall, it may struggle with particular functions.

We now analyze how the dimensionality of a function’s domain influences the effectiveness of transfer learning. For 5D functions (refer to Fig. 10 and Table 2 in the supplementary material [2]), the transferred model significantly outperforms the original GPR across most BBOB functions, regardless of the transfer sample size. However, exceptions are observed in functions F16, F21, and F23. As the transfer data size increases to 40, a growing number of BBOB functions favor models trained from scratch, reducing the relative benefits of transfer learning compared to the 2D scenario. When the

transfer sample size reaches 200, the model trained from scratch significantly outperforms the transferred model on several functions. For instance, on F5, the trained-from-scratch model consistently delivers superior performance, regardless of sample size. Furthermore, for functions such as F16 and F23, the performance of both models remains nearly identical across all sample sizes, showing no improvement despite an increase in the number of transfer samples. This is likely because these functions are inherently tricky for GPR to learn effectively.

For 10D functions (refer to the supplementary material [2]), models trained from scratch struggle with poor performance when sample sizes are small. As dimensionality increases, the complexity of the function landscape requires substantially more data for GPR models to achieve accurate approximations, as previously noted. Under such data-scarce conditions, transfer learning provides a clear advantage over training from scratch. Interestingly, a significant phase transition occurs around 80 samples for the scratch-trained model, marked by a sharp drop in its SMAPE value. This significantly narrows the performance gap with the transferred model. At the largest tested sample size (400), the scratch-trained model outperforms the transferred model across most functions. However, for highly multimodal functions like F16 and F23, transfer learning fails to improve the performance of the original GPR model. In contrast, training the GPR model from scratch with 400 samples achieves superior results on these complex functions. This underscores the limitations of transfer learning in handling highly intricate and multimodal landscapes, where large amounts of task-specific data are essential for optimal performance.

5.2 Ablation study of transferring GPR on BBOB

Fig. 5 shows an ablation study on 2D BBOB functions, analyzing the impact of using only the beta CDF warping function, approximating an exponential transformation without rotation or translation. Results are compared to reproduced code from [24], which uses only affine transformations. The performance is visualized using

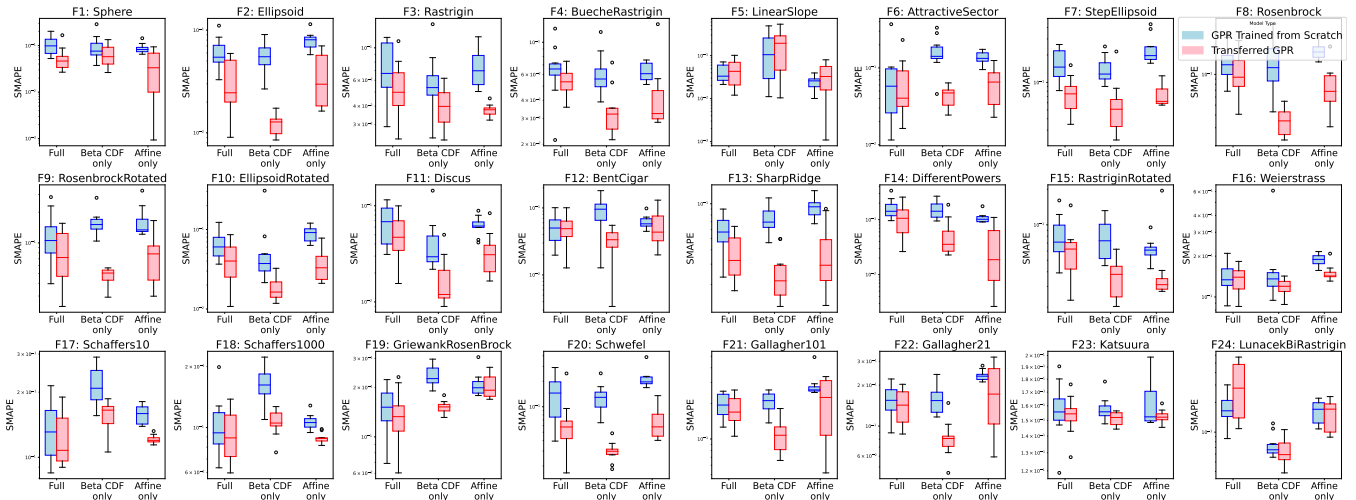


Figure 5: The ablation study focuses on the beta CDF warping function, with rotation and translation disabled, approximating an exponential transformation. We compare our results with reproduced code from [24] using box plots for 2D BBOB functions with a 20-sample transfer dataset. The plots show SMAPE values (*y*-axis) for the transferred GPR and a model trained solely on the transfer dataset across different transfer learning settings (*x*-axis).

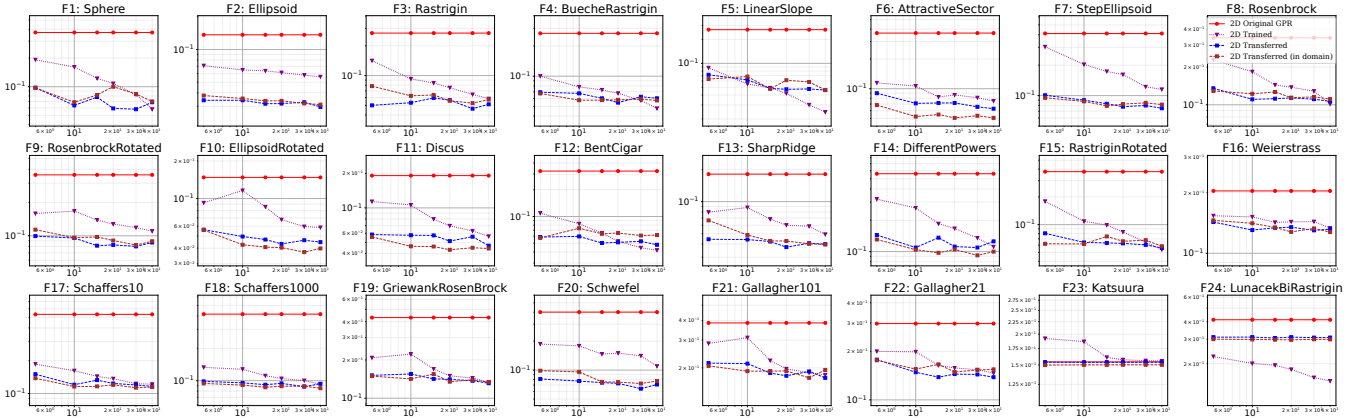


Figure 6: Ablation study presents results for the “in domain” scenario, where only transfer data—sampled from the target domain and mapped back into the original domain after transformation—is used for training. SMAPE values (*y*-axis) are shown for the original GPR, transferred GPR, and a model trained solely on the transfer dataset, plotted against transfer dataset sizes (*x*-axis: 5, 10, 15, 20, 30, 40) for 2D BBOB functions. The analysis combines a beta CDF warping function (approximating an exponential transformation) with an affine transformation.

box plots of raw SMAPE values obtained from 10 repetitions on 2D BBOB functions, with a transfer dataset of 20 samples. These plots compare the transferred GPR and a model trained solely on the transfer dataset. Since the target functions differ across the three settings, the box plot distributions highlight that, for most BBOB functions, optimizing only the beta CDF parameters in the transferred GPR outperforms jointly optimizing beta CDF and affine parameters and optimizing affine parameters alone. This highlights that optimizing additional parameters (“Full”) increases the complexity and difficulty of the problem. Moreover, the transferred model consistently outperforms the model trained from scratch

when optimizing only the beta CDF parameters across nearly all BBOB functions. Fig. 21 (refer to the supplementary material [2]) presents the results for the 5D case, which exhibits a similar pattern to the observations described above.

The inclusion of rotation and translation in the transformations can introduce boundary effects, where parts of the function landscape initially outside the domain are mapped into it after transformation [24]. We also examine the “in-domain” setting, where only transfer data—mapped back to the original domain post-transformation—was used for training. This analysis, presented in Fig. 6, complements the previously examined scenario

of random sampling directly from the target function. This figure demonstrates how model performance varies with different transfer dataset sizes and sampling strategies. For most functions, both “2D Transferred” and “2D Transferred (in the domain)” exhibit decreasing SMAPE values as the number of samples increases, indicating improved performance with more data. Notably, certain functions, such as F6, F10, F11, and even the more challenging ones like F23 and F24, display significant performance gaps between the two models, emphasizing the benefits of staying within the domain. In contrast, for functions such as F2 and F7, the performance of “2D Transferred” and “2D Transferred (in domain)” is nearly identical, suggesting that domain restriction has minimal impact in these cases. Although some functions perform better on “Transferred (in domain)” than “Transferred” under specific transfer dataset sizes, Fig. 22 (see supplementary material [2]) shows that in the 5D case, the difference is minimal, unlike in 2D cases.

5.3 Transferring GPR on real-world benchmark from automobile industry

As highlighted in [25], optimizing with affine transformations has proven effective for many real-world transfer learning applications. However, transferring knowledge between problem instances in the automobile industry presents persistent challenges that require further investigation. We choose this highly challenging benchmark to showcase and evaluate the effectiveness of our transfer learning approach. Fig. 7 (with full results available in Fig. 23, as detailed in the supplementary material [2]) illustrates the SMAPE trends for four GPR models across varying transfer dataset sizes, highlighting a subset of the experimental results. These include the original GPR model, a transferred GPR model that assumes an unknown affine transformation between the source and target problem instances (referred to as “Transferred (Affine only)” [24]), a transferred GPR model leveraging our proposed method (referred to as “Transferred (Full)”), and a model trained solely on the transfer dataset.

Overall, in most cases, the transferred GPR model surpasses the performance of the model trained from scratch, mainly when the transfer dataset is relatively small (fewer than 30 samples). However, as the sample size increases, the performance of the GPR model trained from scratch progressively catches up. Interestingly, there are specific scenarios, such as transferring related to problem instance3, where the transfer learning approach fails. Combined with the instance landscapes discussed in the original study [39], these findings suggest that instance3 differs significantly from the other instances, presenting substantial challenges for effective transfer.

The results demonstrate that our proposed transfer learning method consistently outperforms the affine-only transferred approach across various transfer dataset sizes, particularly in scenarios like transferring from instance1 to instance2. Moreover, the proposed method excels in transfers involving instance3, significantly outperforming the affine-only approach, demonstrating its ability to capture more complex relations between source and target functions. However, the scratch-trained model remains the top performer among all GPR variants, indicating that the relations involving instance3 are still too intricate to fully capture.

In the BBOB problem suite, our target functions are explicitly designed so that a perfect transformation exists—meaning that if we

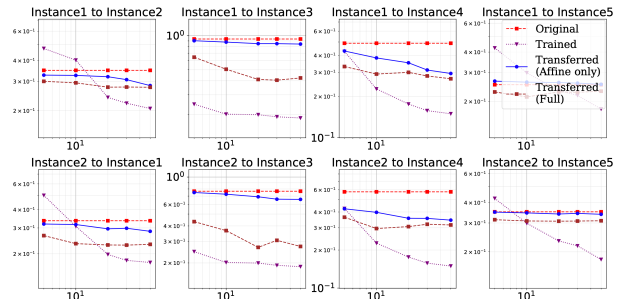


Figure 7: The study evaluates SMAPE values (y -axis) for four GPR models on an automotive industry benchmark (Part of): the original GPR model, a transferred GPR with an assumed affine transformation (“Transferred (Affine only)” [24]), a transferred GPR model using the proposed method (“Transferred (Full)”), and a model trained solely on the transfer dataset. SMAPE values are plotted against transfer dataset sizes (x -axis: 5, 10, 20, 30, and 50).

replicate the settings used to generate the source problem, the resulting model performs equally well on the target problem as it did on the source (disregarding stochastic variations in sampled evaluation points and the influence of out-of-domain samples). However, real-world scenarios rarely offer such guarantees; we typically lack knowledge of any explicit relation between source and target, let alone whether it aligns with our parameterized transformation space. Consequently, there is a tradeoff between the complexity of the transformation and its optimization feasibility, as partially illustrated by our ablation experiment in Fig. 5. Additionally, the original GPR model rarely outperforms the transferred or scratch-trained models, especially when the transfer dataset is extremely small (e.g., five samples). However, occasional exceptions do occur. In such cases, the transferred model may overfit the limited data during optimization, resulting in poor generalization to the broader target domain.

6 CONCLUSION

We present a transfer learning approach to dealing with a complex, nonlinear covariant shift between the source and target problems. We parameterize the unknown covariant shift as the composition of input warping (implemented with beta CDF) and an affine transformation. The method leverages a small transfer dataset drawn on the target problem to learn the covariant shift, enabling an effective surrogate model transfer between problems.

Experiments with BBOB functions demonstrate the effectiveness of the proposed method. With 20-sample transfer datasets, the transferred GPR outperforms models trained from scratch, particularly in 10D settings. However, with more samples, especially in 5D, scratch-trained models eventually surpass transferred models. The benefits of transfer learning are limited for highly complex functions like F16 and F21–F24, where the original GPR struggled with accurate approximation.

The proposed transfer learning method is also validated on a highly challenging real-world automotive task, demonstrating its

effectiveness in low-data scenarios. However, substantial gaps between the source and target domains limit the transfer's effectiveness, even with larger transfer datasets. This highlights the ongoing challenge of adapting the method to different problem instances within the automotive domain and the need for a deeper understanding of their relations.

Future research includes (1) extending this approach to other regression models, such as random forests; (2) integrating active learning into the transfer learning process to sample data points, which will maximally increase the performance; (3) investigating the trade-off between the expressivity of the transformation and the trainability of the transfer learning method.

REFERENCES

- [1] Anestis Antoniadis, Sophie Lambert-Lacroix, and Jean-Michel Poggi. 2021. Random forests for global sensitivity analysis: A selective review. *Reliability Engineering & System Safety* 206 (2021), 107312. doi:10.1016/j.ress.2020.107312
- [2] Anonymous Author(s). 2025. Transfer Learning of Surrogate Models: Integrating Domain Warping and Affine Transformations: Supplementary Material. <https://doi.org/10.5281/zenodo.14728764>.
- [3] Atharv Bhoekar and Marianthi Ilerapetritou. 2018. Advances in surrogate based modeling, feasibility analysis, and optimization: A review. *Computers & Chemical Engineering* 108 (2018), 250–267. doi:10.1016/j.compchemeng.2017.09.017
- [4] Adam D. Bull. 2011. Convergence Rates of Efficient Global Optimization Algorithms. *J. Mach. Learn. Res.* 12 (2011), 2879–2904. doi:10.5555/1953048.2078198
- [5] Bin Cao, Sinno Jialin Pan, Yu Zhang, Dit-Yan Yeung, and Qiang Yang. 2010. Adaptive Transfer Learning. In *Proceedings of the Twenty-Fourth AAAI Conference on Artificial Intelligence, AAAI 2010, Atlanta, Georgia, USA, July 11-15, 2010*, Maria Fox and David Poole (Eds.). AAAI Press, Atlanta, Georgia, USA, 407–412. doi:10.1609/AAAILV24i1.7682
- [6] Yutian Chen, Xingyou Song, Chansoo Lee, Zi Wang, Richard Zhang, David Dohan, Kazuya Kawakami, Greg Kochanski, Arnaud Doucet, Marc'Aurelio Ranzato, Sagi Perel, and Nando de Freitas. 2022. Towards Learning Universal Hyperparameter Optimizers with Transformers. In *Advances in Neural Information Processing Systems*. New Orleans, LA, USA. http://papers.nips.cc/paper_files/paper/2022/hash/cf6501108fcd72ee5c47e2151c4e153-Abstract-Conference.html
- [7] Alexander I Cowen-Rivers, Wenlong Lyu, Rasul Tutunov, Zhi Wang, Antoine Grosnit, Ryan Rhys Griffiths, Alexandre Max Maraval, Hao Jianye, Jun Wang, Jan Peters, et al. 2022. Hebo: Pushing the limits of sample-efficient hyper-parameter optimisation. *Journal of Artificial Intelligence Research* 74 (2022), 1269–1349.
- [8] Bingshui Da, Yew-Soon Ong, Abhishek Gupta, Liang Feng, and Haitao Liu. 2019. Fast transfer Gaussian process regression with large-scale sources. *Knowledge-Based Systems* 165 (2019), 208–218. doi:10.1016/j.knsys.2018.11.029
- [9] Hal Daumé. 2009. Frustratingly Easy Domain Adaptation. *CoRR* abs/0907.1815 (2009). arXiv:0907.1815 <http://arxiv.org/abs/0907.1815>
- [10] Jacob de Nobel, Furong Ye, Diederick Vermetten, Hao Wang, Carola Doerr, and Thomas Bäck. 2024. IOHexperimenter: Benchmarking Platform for Iterative Optimization Heuristics. *Evolutionary Computation* (2024), 1–6. doi:10.1162/evco_a_00342
- [11] Simon S. Du, Jayanth Koushik, Aarti Singh, and Barnabás Póczos. 2017. Hypothesis Transfer Learning via Transformation Functions. In *Advances in Neural Information Processing Systems 30: Annual Conference on Neural Information Processing Systems 2017, December 4-9, 2017, Long Beach, CA, USA*, Isabelle Guyon, Ulrike von Luxburg, Samy Bengio, Hanna M. Wallach, Rob Fergus, S. V. N. Vishwanathan, and Roman Garnett (Eds.). 574–584. <https://proceedings.neurips.cc/paper/2017/hash/352fe25daf686bdb4edca223c921acea-Abstract.html>
- [12] Michael Emmerich, Ofer M. Shir, and Hao Wang. 2018. Evolution Strategies. In *Handbook of Heuristics*, Rafael Martí, Panos M. Pardalos, and Mauricio G. C. Resende (Eds.). Springer, 89–119. doi:10.1007/978-3-319-07124-4_13
- [13] Jianguang Fang, Guangyong Sun, Na Qiu, Nam H Kim, and Qing Li. 2017. On design optimization for structural crashworthiness and its state of the art. *Structural and Multidisciplinary Optimization* 55 (2017), 1091–1119.
- [14] Benito E. Flores. 1986. A pragmatic view of accuracy measurement in forecasting. *Omega* 14, 2 (1986), 93–98.
- [15] Alexander J Forrester and Andy J Keane. 2009. Recent advances in surrogate-based optimization. *Progress in aerospace sciences* 45, 1-3 (2009), 50–79.
- [16] Alexander I. J. Forrester, Andras Sobester, and Andy J. Keane. 2008. *Engineering Design via Surrogate Modelling - A Practical Guide*. Wiley. doi:10.1002/9780470770801
- [17] Nikolaus Hansen. 2006. The CMA Evolution Strategy: A Comparing Review. In *Towards a New Evolutionary Computation - Advances in the Estimation of Distribution Algorithms*, José Antonio Lozano, Pedro Larrañaga, Inaki Inza, and Endika Bengoetxea (Eds.). Studies in Fuzziness and Soft Computing, Vol. 192. Springer, 75–102. doi:10.1007/3-540-32494-1_4
- [18] Nikolaus Hansen. 2016. The CMA Evolution Strategy: A Tutorial. *CoRR* abs/1604.00772 (2016). arXiv:1604.00772 <http://arxiv.org/abs/1604.00772>
- [19] Nikolaus Hansen, Anne Auger, Raymond Ros, Olaf Mersmann, Tea Tušar, and Dimo Brockhoff. 2020. COCO: A platform for comparing continuous optimizers in a black-box setting. *Optimization Methods and Software* 36, 1 (2020), 1–31. doi:10.1080/10556788.2020.1808977
- [20] Nikolaus Hansen, Steffen Finck, Raymond Ros, and Anne Auger. 2009. *Real-Parameter Black-Box Optimization Benchmarking 2009: Noiseless Functions Definitions*. Technical Report RR-6829. INRIA, France. Updated February 2010.
- [21] Nikolaus Hansen, Steffen Finck, Raymond Ros, and Anne Auger. 2009. *Real-Parameter Black-Box Optimization Benchmarking 2009: Noiseless Functions Definitions*. Research Report RR-6829. INRIA. <https://hal.inria.fr/inria-00362633/document>
- [22] Morteza Kiani and Ali R Yildiz. 2016. A comparative study of non-traditional methods for vehicle crashworthiness and NVH optimization. *Archives of Computational Methods in Engineering* 23 (2016), 723–734.
- [23] Marius Thomas Lindauer, Katharina Eggensperger, Matthias Feurer, André Biedenkapp, Difan Deng, Carolin Benjamins, Tim Ruhkopf, René Sass, and Frank Hutter. 2022. SMAC3: A Versatile Bayesian Optimization Package for Hyperparameter Optimization. *Journal of Machine Learning Research* 23 (2022), 1–9.
- [24] Shuaiqun Pan, Diederick Vermetten, Manuel López-Ibáñez, Thomas Bäck, and Hao Wang. 2024. Transfer Learning of Surrogate Models via Domain Affine Transformation. In *Proceedings of the Genetic and Evolutionary Computation Conference, GECCO 2024, Julia Handl and Xiaodong Li (Eds.)*. ACM Press, New York, NY. doi:10.1145/3638529.3654032
- [25] Shuaiqun Pan, Diederick Vermetten, Manuel López-Ibáñez, Thomas Bäck, and Hao Wang. 2025. Transfer Learning of Surrogate Models via Domain Affine Transformation Across Synthetic and Real-World Benchmarks. arXiv:2501.14012 [cs.LG] <https://arxiv.org/abs/2501.14012>
- [26] Sinno Jialin Pan and Qiang Yang. 2010. A Survey on Transfer Learning. *IEEE Trans. Knowl. Data Eng.* 22, 10 (2010), 1345–1359. doi:10.1109/TKDE.2009.191
- [27] Milan Papez and Anthony Quinn. 2022. Transferring model structure in Bayesian transfer learning for Gaussian process regression. *Knowl. Based Syst.* 251 (2022), 108875. doi:10.1016/j.knsys.2022.108875
- [28] Reese Pathak, Cong Ma, and Martin J. Wainwright. 2022. A new similarity measure for covariate shift with applications to nonparametric regression. In *International Conference on Machine Learning, ICML 2022, 17-23 July 2022, Baltimore, Maryland, USA (Proceedings of Machine Learning Research, Vol. 162)*, Kamalika Chaudhuri, Stefanie Jegelka, Le Song, Csaba Szepesvári, Gang Niu, and Sivan Sabato (Eds.). PMLR, 17517–17530. <https://proceedings.mlr.press/v162/pathak22a.html>
- [29] Tony Pourmohamad. 2021. Surrogates: Gaussian Process Modeling, Design, and Optimization for the Applied Sciences. *Technometrics* 63, 1 (2021), 144–145. doi:10.1080/00401706.2020.1865008
- [30] Na Qiu, Yunkai Gao, Jianguang Fang, Guangyong Sun, Qing Li, and Nam H Kim. 2018. Crashworthiness optimization with uncertainty from surrogate model and numerical error. *Thin-Walled Structures* 129 (2018), 457–472.
- [31] Dushyanth Rajaram, Tejas G Puranik, Ashwin Renganathan, Woong Je Sung, Olivia J Pinon-Fischer, Dimitri N Mavris, and Arun Ramamurthy. 2020. Deep Gaussian process enabled surrogate models for aerodynamic flows. In *AIAA scitech 2020 forum*. 1640.
- [32] Danilo Jimenez Rezende and Shakir Mohamed. 2015. Variational Inference with Normalizing Flows. In *Proceedings of the 32nd International Conference on Machine Learning, ICML 2015, Lille, France, 6-11 July 2015 (JMLR Workshop and Conference Proceedings, Vol. 37)*, Francis R. Bach and David M. Blei (Eds.). JMLR.org, 1530–1538. <http://proceedings.mlr.press/v37/rezende15.html>
- [33] Taisei Saida and Mayuko Nishio. 2023. Transfer learning Gaussian process regression surrogate model with explainability for structural reliability analysis under variation in uncertainties. *Computers & Structures* 281 (2023), 107014.
- [34] Pramudita Satria Palar, Lavi Rizki Zuhail, and Koji Shimoyama. 2020. Gaussian process surrogate model with composite kernel learning for engineering design. *AIAA journal* 58, 4 (2020), 1864–1880.
- [35] Hidetoshi Shimodaira. 2000. Improving predictive inference under covariate shift by weighting the log-likelihood function. *Journal of Statistical Planning and Inference* 90, 2 (2000), 227–244. doi:10.1016/S0378-3758(00)00115-4
- [36] Priyanka Singh and Pragna Dwivedi. 2018. Integration of new evolutionary approach with artificial neural network for solving short term load forecast problem. *Applied energy* 217 (2018), 537–549.
- [37] Jasper Snoek, Kevin Swersky, Rich Zemel, and Ryan Adams. 2014. Input Warping for Bayesian Optimization of Non-Stationary Functions. In *Proceedings of the 31st International Conference on Machine Learning (Proceedings of Machine Learning Research, Vol. 32)*, Eric P. Xing and Tony Jebara (Eds.). PMLR, Beijing, China, 1674–1682.
- [38] Masashi Sugiyama, Matthias Krauledat, and Klaus-Robert Müller. 2007. Covariate Shift Adaptation by Importance Weighted Cross Validation. *J. Mach. Learn. Res.* 8 (2007), 985–1005. doi:10.5555/1314498.1390324

- [39] André Thomaser, Marc-Eric Vogt, Thomas Bäck, and Anna V. Kononova. 2023. Real-World Optimization Benchmark from Vehicle Dynamics: Specification of Problems in 2D and Methodology for Transferring (Meta-)Optimized Algorithm Parameters. In *Proceedings of the 15th International Joint Conference on Computational Intelligence, IJCCI 2023, Rome, Italy, November 13-15, 2023*, Niki van Stein, Francesco Marcelloni, H. K. Lam, Marie Cottrell, and Joaquim Filipe (Eds.). SCITEPRESS, 31–40. doi:10.5220/0012158000003595
- [40] Ye Tian, Shichen Peng, Xingyi Zhang, Tobias Rodemann, Kay Chen Tan, and Yaochu Jin. 2020. A Recommender System for Metaheuristic Algorithms for Continuous Optimization Based on Deep Recurrent Neural Networks. *IEEE Transactions on Artificial Intelligence* 1, 1 (2020), 5–18. doi:10.1109/TAI.2020.3022339
- [41] Hao Tong, Changwu Huang, Leandro L. Minku, and Xin Yao. 2021. Surrogate models in evolutionary single-objective optimization: A new taxonomy and experimental study. *Information Sciences* 562 (2021), 414–437. doi:10.1016/j.ins.2021.03.002
- [42] Aad W. Van Der Vaart and J. Harry Van Zanten. 2008. Rates of Contraction of Posterior Distributions Based on Gaussian Process Priors. *The Annals of Statistics* 36, 3 (2008), 1435–1463.
- [43] Handing Wang and Yaochu Jin. 2020. A Random Forest-Assisted Evolutionary Algorithm for Data-Driven Constrained Multiobjective Combinatorial Optimization of Trauma Systems. *IEEE Transactions on Cybernetics* 50, 2 (2020), 536–549. doi:10.1109/TCYB.2018.2869674
- [44] Pengfei Wei, Thanh Vinh Vo, Xinghua Qu, Yew Soon Ong, and Zejun Ma. 2023. Transfer Kernel Learning for Multi-Source Transfer Gaussian Process Regression. *IEEE Transactions on Pattern Analysis and Machine Intelligence* 45, 3 (2023), 3862–3876. doi:10.1109/TPAMI.2022.3184696
- [45] Karl R. Weiss, Taghi M. Khoshgoftaar, and Dingding Wang. 2016. A survey of transfer learning. *J. Big Data* 3 (2016), 9. doi:10.1186/S40537-016-0043-6
- [46] Kaifeng Yang and Michael Affenzeller. 2023. Surrogate-assisted Multi-objective Optimization via Genetic Programming Based Symbolic Regression. In *Evolutionary Multi-Criterion Optimization - 12th International Conference, EMO 2023, Leiden, The Netherlands, March 20-24, 2023, Proceedings (Lecture Notes in Computer Science, Vol. 13970)*, Michael Emmerich, André H. Deutz, Hao Wang, Anna V. Kononova, Boris Naujoks, Ke Li, Kaisa Miettinen, and Iryna Yevseyeva (Eds.). Springer, 176–190. doi:10.1007/978-3-031-27250-9_13
- [47] Xi Zhang, Guo Yu, Yaochu Jin, and Feng Qian. 2023. An adaptive Gaussian process based manifold transfer learning to expensive dynamic multi-objective optimization. *Neurocomputing* 538 (2023), 126212. doi:10.1016/j.neucom.2023.03.073
- [48] Xiubin Zhu, Dan Wang, Witold Pedrycz, and Zhiwu Li. 2023. Transfer Learning Realized With Nonlinearly Transformed Input Space. *IEEE Trans. Emerg. Top. Comput.* 11, 2 (2023), 448–460. doi:10.1109/TETC.2022.3210568
- [49] Fuzhen Zhuang, Zhiyuan Qi, Keyu Duan, Dongbo Xi, Yongchun Zhu, Hengshu Zhu, Hui Xiong, and Qing He. 2021. A Comprehensive Survey on Transfer Learning. *Proc. IEEE* 109, 1 (2021), 43–76. doi:10.1109/JPROC.2020.3004555

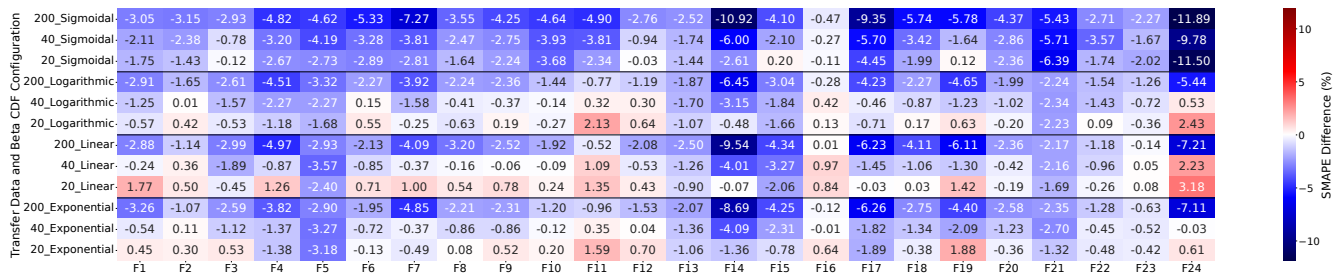


Figure 8: On 5D BBOB functions, we compare the transferred GPR models with those trained from scratch on the transfer dataset. Each cell displays the percentage difference in average SMAPE (%) for a combination of BBOB functions, sample size, and beta CDF shape. Positive values (shown in red) indicate superior performance of the transferred model and vice versa.

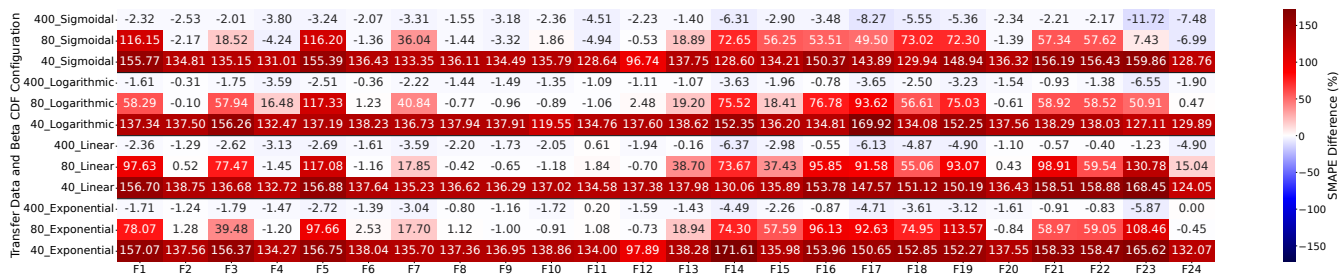


Figure 9: On 10D BBOB functions, we compare the transferred GPR models with those trained from scratch on the transfer dataset. Each cell displays the percentage difference in average SMAPE (%) for a combination of BBOB functions, sample size, and beta CDF shape. Positive values (shown in red) indicate superior performance of the transferred model and vice versa.

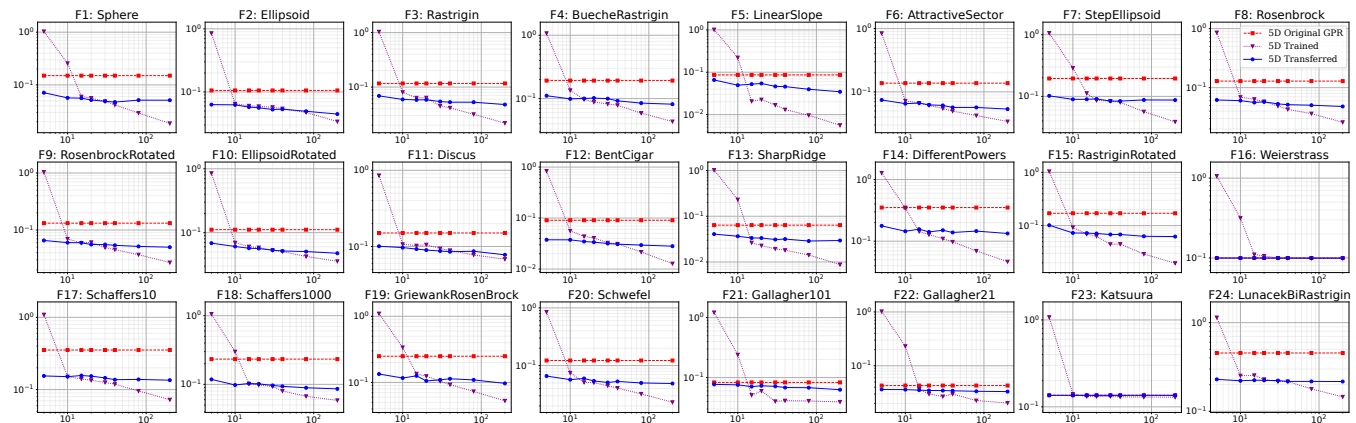


Figure 10: The SMAPE values (y -axis) for the original GPR, transferred GPR, and GPR trained solely on the transfer dataset are plotted against the transfer dataset sizes (x -axis: 5, 10, 15, 20, 30, 40, 80, 200) for 5D BBOB functions. The analysis combines a beta CDF warping function (approximating an exponential transformation) with an affine transformation.

5D	Original GPR	Train from scratch	Transferred	Train from scratch	Transferred	Train from scratch	Transferred
		20 samples		40 samples		200 samples	
F1	0.1499 ± 0.0409	0.0562 ± 0.0186	<u>0.0517 ± 0.0112</u>	0.0418 ± 0.0112	<u>0.0472 ± 0.0123</u>	0.0186 ± 0.0057	<u>0.0512 ± 0.0125</u>
F2	0.1058 ± 0.0137	0.0592 ± 0.0168	<u>0.0562 ± 0.0148</u>	0.0545 ± 0.0165	<u>0.0534 ± 0.0166</u>	0.0340 ± 0.0081	<u>0.0447 ± 0.0126</u>
F3	0.1165 ± 0.0337	0.0637 ± 0.0218	<u>0.0584 ± 0.0134</u>	0.0416 ± 0.0154	<u>0.0528 ± 0.0087</u>	0.0218 ± 0.0068	<u>0.0477 ± 0.0047</u>
F4	0.1924 ± 0.0537	0.0882 ± 0.0188	<u>0.1020 ± 0.0197</u>	0.0784 ± 0.0180	<u>0.0921 ± 0.0126</u>	0.0434 ± 0.0075	<u>0.0816 ± 0.0162</u>
F5	0.0865 ± 0.0284	0.0226 ± 0.0134	<u>0.0544 ± 0.0340</u>	0.0131 ± 0.0079	<u>0.0458 ± 0.0139</u>	0.0056 ± 0.0033	<u>0.0346 ± 0.0072</u>
F6	0.1374 ± 0.0290	0.0611 ± 0.0226	<u>0.0624 ± 0.0222</u>	0.0496 ± 0.0254	<u>0.0568 ± 0.0241</u>	0.0340 ± 0.0190	<u>0.0535 ± 0.0192</u>
F7	0.1952 ± 0.0362	0.0860 ± 0.0262	<u>0.0909 ± 0.0163</u>	0.0802 ± 0.0227	<u>0.0839 ± 0.0204</u>	0.0387 ± 0.0101	<u>0.0872 ± 0.0138</u>
F8	0.1291 ± 0.0129	0.0583 ± 0.0108	<u>0.0575 ± 0.0087</u>	0.0429 ± 0.0052	<u>0.0515 ± 0.0059</u>	0.0259 ± 0.0037	<u>0.0480 ± 0.0087</u>
F9	0.1319 ± 0.0238	0.0608 ± 0.0195	<u>0.0556 ± 0.0093</u>	0.0453 ± 0.0111	<u>0.0539 ± 0.0093</u>	0.0269 ± 0.0046	<u>0.0500 ± 0.0065</u>
F10	0.1114 ± 0.0156	0.0585 ± 0.0216	<u>0.0565 ± 0.0197</u>	0.0505 ± 0.0222	<u>0.0517 ± 0.0163</u>	0.0356 ± 0.0142	<u>0.0476 ± 0.0159</u>
F11	0.1504 ± 0.0191	0.1056 ± 0.0344	<u>0.0897 ± 0.0255</u>	0.0889 ± 0.0245	<u>0.0854 ± 0.0269</u>	0.0682 ± 0.0196	<u>0.0778 ± 0.0285</u>
F12	0.0906 ± 0.0426	0.0407 ± 0.0072	<u>0.0337 ± 0.0107</u>	0.0312 ± 0.0104	<u>0.0308 ± 0.0070</u>	0.0128 ± 0.0021	<u>0.0281 ± 0.0080</u>
F13	0.0639 ± 0.0152	0.0228 ± 0.0078	<u>0.0334 ± 0.0093</u>	0.0181 ± 0.0085	<u>0.0317 ± 0.0068</u>	0.0088 ± 0.0037	<u>0.0295 ± 0.0073</u>
F14	0.3513 ± 0.0437	0.1279 ± 0.0457	<u>0.1415 ± 0.0331</u>	0.0976 ± 0.0347	<u>0.1385 ± 0.0337</u>	0.0465 ± 0.0145	<u>0.1334 ± 0.0331</u>
F15	0.1704 ± 0.0337	0.0631 ± 0.0286	<u>0.0709 ± 0.0218</u>	0.0449 ± 0.0261	<u>0.0680 ± 0.0166</u>	0.0196 ± 0.0099	<u>0.0621 ± 0.0149</u>
F16	0.0999 ± 0.0019	0.1061 ± 0.0198	0.0997 ± 0.0020	0.0996 ± 0.0020	0.0997 ± 0.0020	0.0985 ± 0.0021	0.0997 ± 0.0020
F17	0.3530 ± 0.0759	0.1346 ± 0.0242	<u>0.1535 ± 0.0353</u>	0.1189 ± 0.0219	<u>0.1371 ± 0.0244</u>	0.0724 ± 0.0093	<u>0.1350 ± 0.0370</u>
F18	0.2331 ± 0.0617	0.0979 ± 0.0195	<u>0.1017 ± 0.0200</u>	0.0802 ± 0.0142	<u>0.0936 ± 0.0183</u>	0.0585 ± 0.0077	<u>0.0860 ± 0.0184</u>
F19	0.2491 ± 0.0486	0.1243 ± 0.0234	<u>0.1055 ± 0.0100</u>	0.0928 ± 0.0139	<u>0.1137 ± 0.0195</u>	0.0528 ± 0.0120	<u>0.0968 ± 0.0129</u>
F20	0.1225 ± 0.0254	0.0506 ± 0.0154	<u>0.0542 ± 0.0130</u>	0.0408 ± 0.0146	<u>0.0531 ± 0.0127</u>	0.0231 ± 0.0084	<u>0.0489 ± 0.0152</u>
F21	0.0830 ± 0.0052	0.0598 ± 0.0380	<u>0.0730 ± 0.0154</u>	0.0412 ± 0.0130	<u>0.0682 ± 0.0134</u>	0.0393 ± 0.0124	<u>0.0628 ± 0.0097</u>
F22	0.0430 ± 0.0028	0.0300 ± 0.0105	<u>0.0348 ± 0.0068</u>	0.0299 ± 0.0154	<u>0.0344 ± 0.0071</u>	0.0204 ± 0.0047	<u>0.0332 ± 0.0064</u>
F23	0.1361 ± 0.0026	0.1314 ± 0.0070	<u>0.1356 ± 0.0028</u>	0.1303 ± 0.0061	<u>0.1355 ± 0.0028</u>	0.1292 ± 0.0061	<u>0.1355 ± 0.0028</u>
F24	0.4548 ± 0.1174	0.2294 ± 0.0394	<u>0.2233 ± 0.0292</u>	0.2171 ± 0.0418	<u>0.2174 ± 0.0281</u>	0.1456 ± 0.0148	<u>0.2167 ± 0.0265</u>

Table 2: On 5D BBOB functions, we compare the SMAPE value (mean ± standard deviation) of three GPR models: the original model, the transferred model, and the one trained from scratch on the transfer dataset. Three transfer sample sizes are investigated $|\mathcal{T}| \in \{20, 40, 200\}$. The transfer target is created with an exponential-shaped beta CDF. We apply the Kruskal-Wallis test with a significance level of 5%, followed by Dunn’s posthoc analysis to detect significant winners: the transferred model has underlined if it outperforms the original model; the boldface indicates the better one between the transferred and the model trained from scratch.

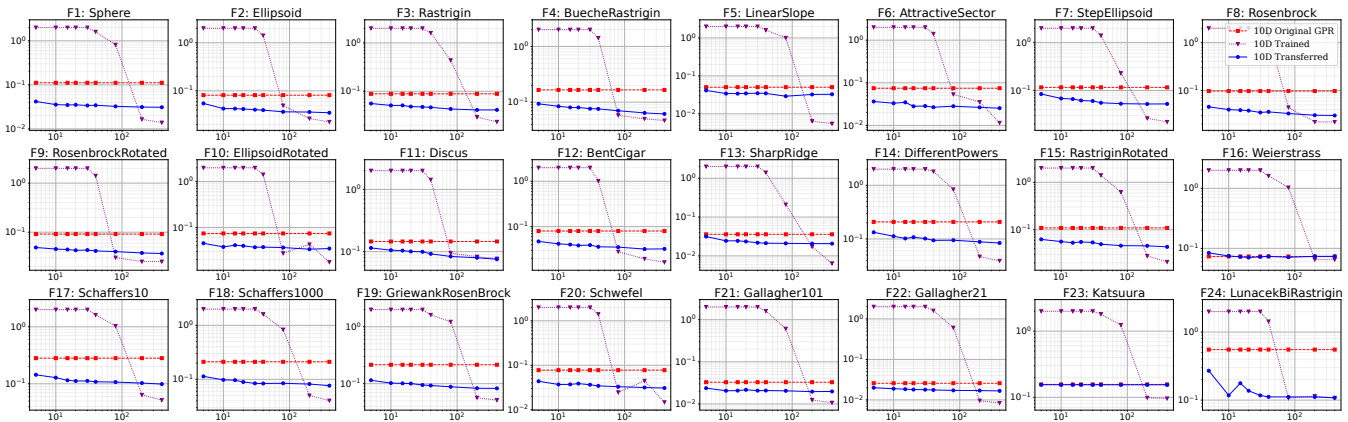


Figure 11: The SMAPE values (y -axis) for the original GPR, transferred GPR, and GPR trained solely on the transfer dataset are plotted against the transfer dataset sizes (x -axis: 5, 10, 15, 20, 30, 40, 80, 200, 400) for 10D BBOB functions. The analysis combines a beta CDF warping function (approximating an exponential transformation) with an affine transformation.

10D	Original GPR	Train from scratch		Transferred		Train from scratch		Transferred	
		40 samples				80 samples			
F1	0.1116 ± 0.0286	1.6051 ± 0.7898	<u>0.0344 ± 0.0091</u>	0.8132 ± 0.9690	<u>0.0325 ± 0.0082</u>	0.0139 ± 0.0033	<u>0.0310 ± 0.0071</u>		
F2	0.0812 ± 0.0139	1.4153 ± 0.8932	<u>0.0397 ± 0.0117</u>	0.0494 ± 0.0326	<u>0.0366 ± 0.0089</u>	0.0226 ± 0.0080	<u>0.0350 ± 0.0080</u>		
F3	0.0887 ± 0.0219	1.6102 ± 0.7796	<u>0.0465 ± 0.0103</u>	0.4379 ± 0.7816	<u>0.0431 ± 0.0099</u>	0.0234 ± 0.0053	<u>0.0413 ± 0.0104</u>		
F4	0.1661 ± 0.0531	1.4185 ± 0.8881	<u>0.0758 ± 0.0147</u>	0.0583 ± 0.0100	<u>0.0703 ± 0.0125</u>	0.0469 ± 0.0101	<u>0.0616 ± 0.0106</u>		
F5	0.0503 ± 0.0097	1.6021 ± 0.7957	<u>0.0346 ± 0.0131</u>	1.0057 ± 0.9942	<u>0.0291 ± 0.0064</u>	0.0055 ± 0.0020	<u>0.0327 ± 0.0094</u>		
F6	0.0745 ± 0.0109	1.4071 ± 0.9056	<u>0.0267 ± 0.0095</u>	0.0535 ± 0.0668	<u>0.0282 ± 0.0118</u>	0.0115 ± 0.0063	<u>0.0254 ± 0.0097</u>		
F7	0.1161 ± 0.0113	1.4123 ± 0.8978	<u>0.0553 ± 0.0119</u>	0.2300 ± 0.5901	<u>0.0530 ± 0.0111</u>	0.0220 ± 0.0080	<u>0.0524 ± 0.0092</u>		
F8	0.0971 ± 0.0330	1.4093 ± 0.9023	<u>0.0357 ± 0.0059</u>	0.0442 ± 0.0344	<u>0.0330 ± 0.0059</u>	0.0220 ± 0.0157	<u>0.0300 ± 0.0052</u>		
F9	0.0916 ± 0.0187	1.4111 ± 0.8995	<u>0.0416 ± 0.0062</u>	0.0303 ± 0.0069	<u>0.0403 ± 0.0048</u>	0.0252 ± 0.0127	<u>0.0368 ± 0.0030</u>		
F10	0.0742 ± 0.0129	1.4260 ± 0.8782	<u>0.0374 ± 0.0098</u>	0.0275 ± 0.0106	<u>0.0366 ± 0.0089</u>	0.0176 ± 0.0065	<u>0.0348 ± 0.0086</u>		
F11	0.1458 ± 0.0088	1.4323 ± 0.8671	<u>0.0923 ± 0.0206</u>	0.0946 ± 0.0177	<u>0.0838 ± 0.0186</u>	0.0775 ± 0.0286	<u>0.0755 ± 0.0175</u>		
F12	0.0799 ± 0.0145	1.0147 ± 0.9853	<u>0.0358 ± 0.0050</u>	0.0279 ± 0.0029	<u>0.0352 ± 0.0054</u>	0.0163 ± 0.0026	<u>0.0322 ± 0.0047</u>		
F13	0.0359 ± 0.0055	1.4040 ± 0.9103	<u>0.0212 ± 0.0035</u>	0.2104 ± 0.5965	<u>0.0210 ± 0.0042</u>	0.0064 ± 0.0019	<u>0.0207 ± 0.0041</u>		
F14	0.2082 ± 0.0191	1.8103 ± 0.5689	<u>0.0942 ± 0.0214</u>	0.8378 ± 0.9489	<u>0.0948 ± 0.0174</u>	0.0392 ± 0.0127	<u>0.0841 ± 0.0166</u>		
F15	0.1094 ± 0.0404	1.4094 ± 0.9021	<u>0.0496 ± 0.0093</u>	0.6220 ± 0.9021	<u>0.0461 ± 0.0066</u>	0.0210 ± 0.0042	<u>0.0436 ± 0.0066</u>		
F16	0.0733 ± 0.0132	1.6131 ± 0.7737	<u>0.0735 ± 0.0142</u>	1.0326 ± 0.9673	<u>0.0713 ± 0.0077</u>	0.0648 ± 0.0024	<u>0.0735 ± 0.0144</u>		
F17	0.2814 ± 0.0507	1.6151 ± 0.7698	<u>0.1086 ± 0.0220</u>	1.0335 ± 0.9665	<u>0.1072 ± 0.0180</u>	0.0518 ± 0.0124	<u>0.0989 ± 0.0157</u>		
F18	0.2117 ± 0.0391	1.6123 ± 0.7754	<u>0.0838 ± 0.0185</u>	0.8340 ± 0.9520	<u>0.0845 ± 0.0157</u>	0.0404 ± 0.0064	<u>0.0765 ± 0.0133</u>		
F19	0.2152 ± 0.0457	1.6156 ± 0.7687	<u>0.0929 ± 0.0084</u>	1.2239 ± 0.9504	<u>0.0882 ± 0.0063</u>	0.0515 ± 0.0189	<u>0.0827 ± 0.0064</u>		
F20	0.0776 ± 0.0104	1.4099 ± 0.9014	<u>0.0344 ± 0.0059</u>	0.0246 ± 0.0062	<u>0.0330 ± 0.0058</u>	0.0147 ± 0.0032	<u>0.0308 ± 0.0057</u>		
F21	0.0328 ± 0.0083	1.6041 ± 0.7917	<u>0.0208 ± 0.0045</u>	0.6102 ± 0.9098	<u>0.0205 ± 0.0046</u>	0.0107 ± 0.0007	<u>0.0198 ± 0.0043</u>		
F22	0.0258 ± 0.0068	1.6023 ± 0.7953	<u>0.0176 ± 0.0046</u>	0.6077 ± 0.9114	<u>0.0172 ± 0.0044</u>	0.0084 ± 0.0007	<u>0.0167 ± 0.0042</u>		
F23	0.1566 ± 0.0218	1.8111 ± 0.5667	<u>0.1549 ± 0.0203</u>	1.2393 ± 0.9316	<u>0.1547 ± 0.0203</u>	0.0961 ± 0.0115	<u>0.1548 ± 0.0202</u>		
F24	0.5525 ± 0.0623	1.4323 ± 0.8672	<u>0.1116 ± 0.0305</u>	0.1069 ± 0.0357	<u>0.1114 ± 0.0295</u>	0.1081 ± 0.0290	<u>0.1081 ± 0.0290</u>		

Table 3: On 10D BBOB functions, we compare the SMAPE value (mean ± standard deviation) of three GPR models: the original model, the transferred model, and the one trained from scratch on the transfer dataset. Three transfer sample sizes are investigated $|\mathcal{T}| \in \{40, 80, 400\}$. The transfer target is created with an exponential-shaped beta CDF. We apply the Kruskal-Wallis test with a significance level of 5%, followed by Dunn’s posthoc analysis to detect significant winners: the transferred model is underlined if it outperforms the original model; the boldface indicates the better one between the transferred and the model trained from scratch.

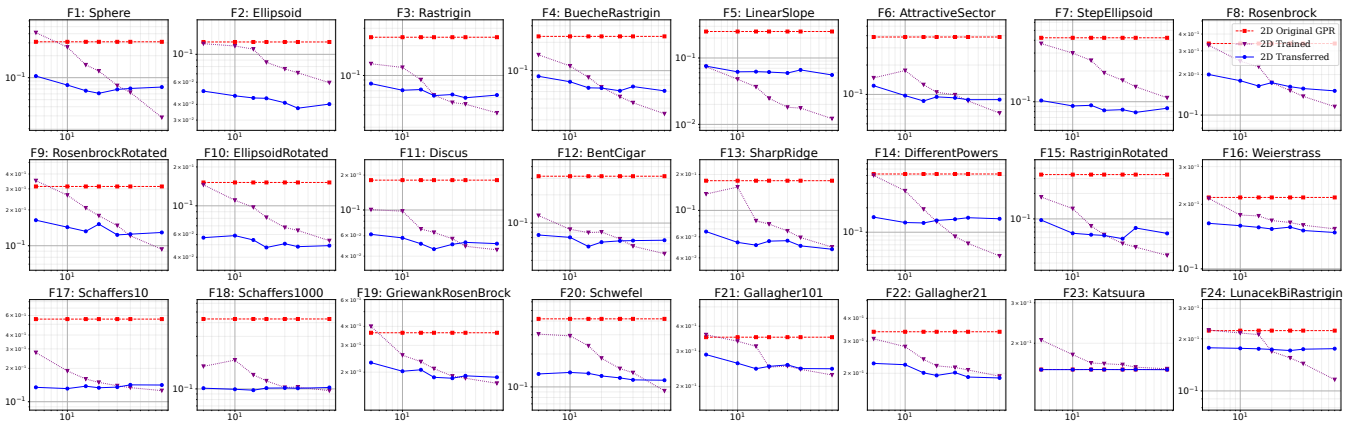


Figure 12: The SMAPE values (y -axis) for the original GPR, transferred GPR, and GPR trained solely on the transfer dataset are plotted against the transfer dataset sizes (x -axis: 5, 10, 15, 20, 30, 40, 80) for 2D BBOB functions. The analysis combines a beta CDF warping function (approximating a linear transformation) with an affine transformation.

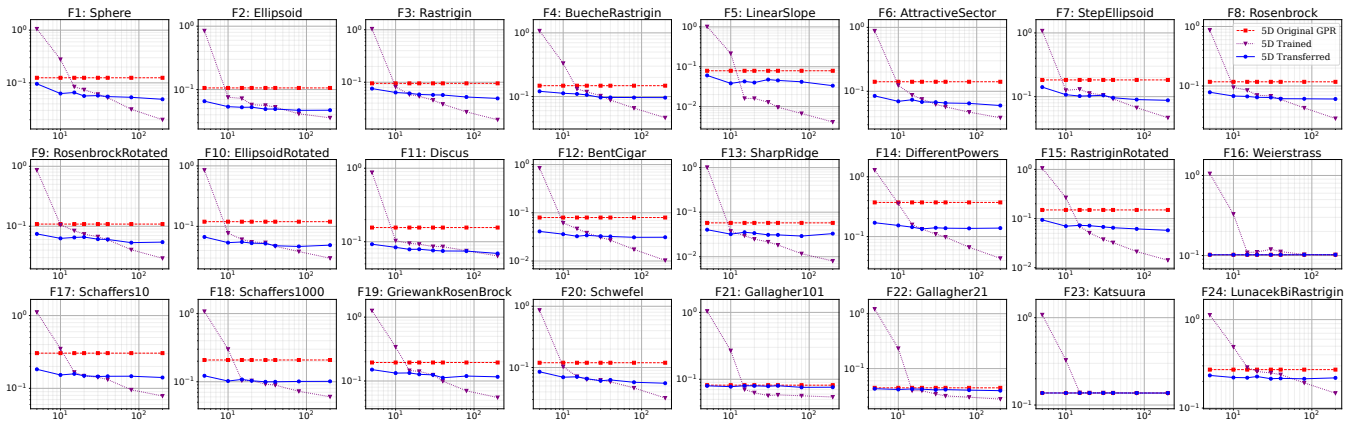


Figure 13: The SMAPE values (y -axis) for the original GPR, transferred GPR, and GPR trained solely on the transfer dataset are plotted against the transfer dataset sizes (x -axis: 5, 10, 15, 20, 30, 40, 80, 200) for 5D BBOB functions. The analysis combines a beta CDF warping function (approximating a linear transformation) with an affine transformation.

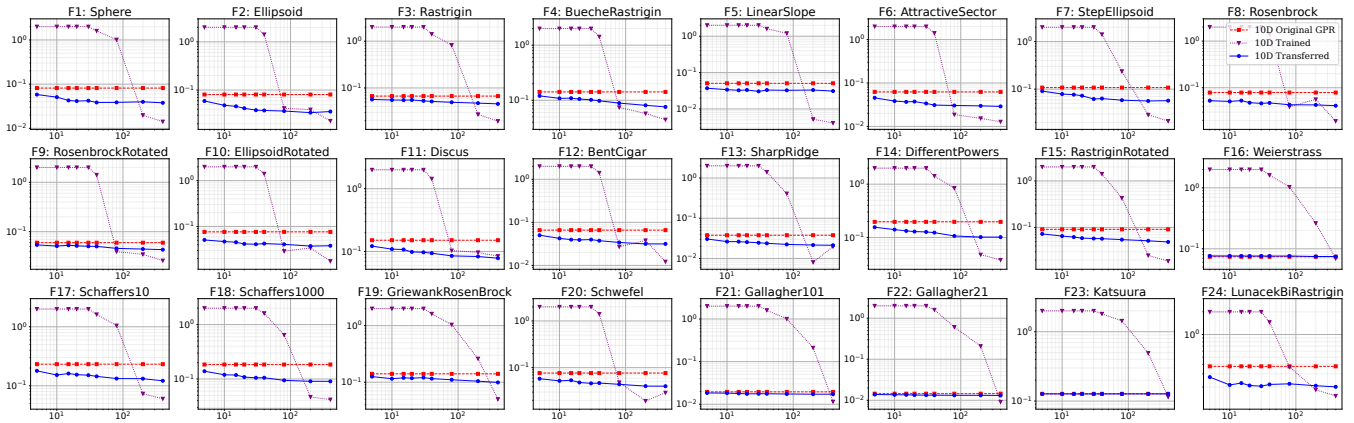


Figure 14: The SMAPE values (y -axis) for the original GPR, transferred GPR, and GPR trained solely on the transfer dataset are plotted against the transfer dataset sizes (x -axis: 5, 10, 15, 20, 30, 40, 80, 200, 400) for 10D BBOB functions. The analysis combines a beta CDF warping function (approximating a linear transformation) with an affine transformation.

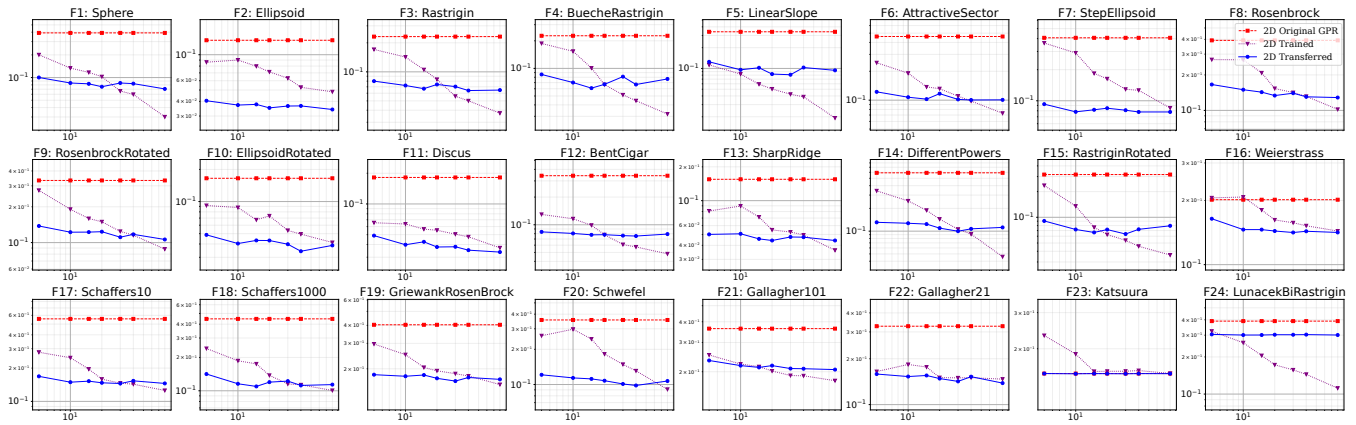


Figure 15: The SMAPE values (y -axis) for the original GPR, transferred GPR, and GPR trained solely on the transfer dataset are plotted against the transfer dataset sizes (x -axis: 5, 10, 15, 20, 30, 40, 80) for 2D BBOB functions. The analysis combines a beta CDF warping function (approximating a logarithmic transformation) with an affine transformation.

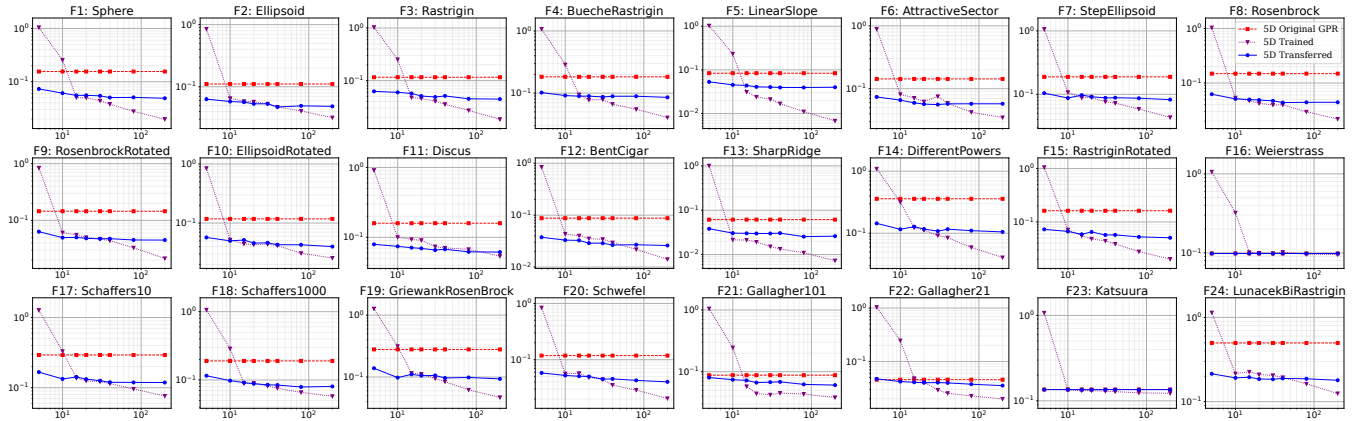


Figure 16: The SMAPE values (y -axis) for the original GPR, transferred GPR, and GPR trained solely on the transfer dataset are plotted against the transfer dataset sizes (x -axis: 5, 10, 15, 20, 30, 40, 80, 200) for 5D BBOB functions. The analysis combines a beta CDF warping function (approximating a logarithmic transformation) with an affine transformation.

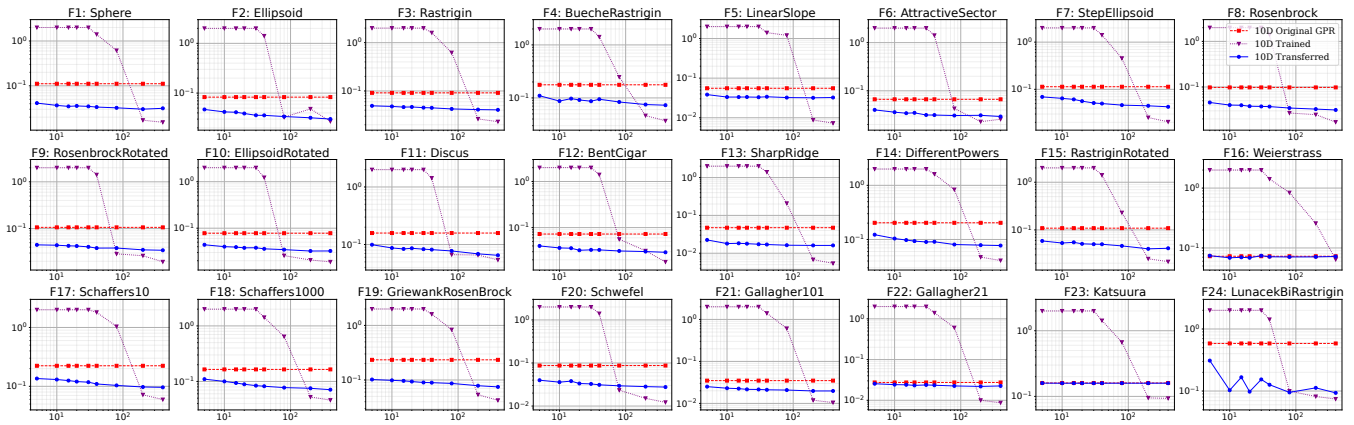


Figure 17: The SMAPE values (y -axis) for the original GPR, transferred GPR, and GPR trained solely on the transfer dataset are plotted against the transfer dataset sizes (x -axis: 5, 10, 15, 20, 30, 40, 80, 200, 400) for 10D BBOB functions. The analysis combines a beta CDF warping function (approximating a logarithmic transformation) with an affine transformation.

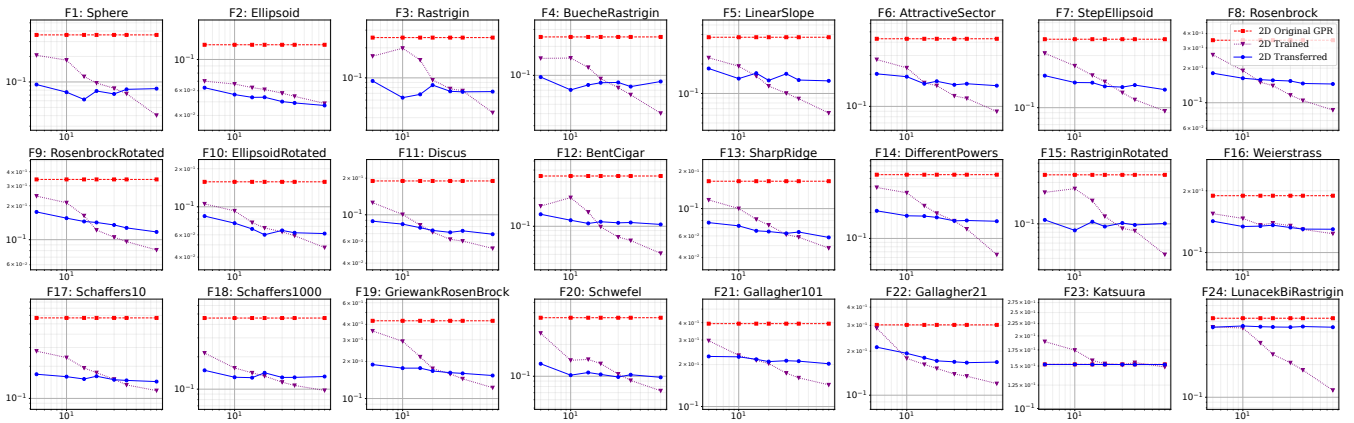


Figure 18: The SMAPE values (y -axis) for the original GPR, transferred GPR, and GPR trained solely on the transfer dataset are plotted against the transfer dataset sizes (x -axis: 5, 10, 15, 20, 30, 40, 80) for 2D BBOB functions. The analysis combines a beta CDF warping function (approximating a sigmoidal transformation) with an affine transformation.

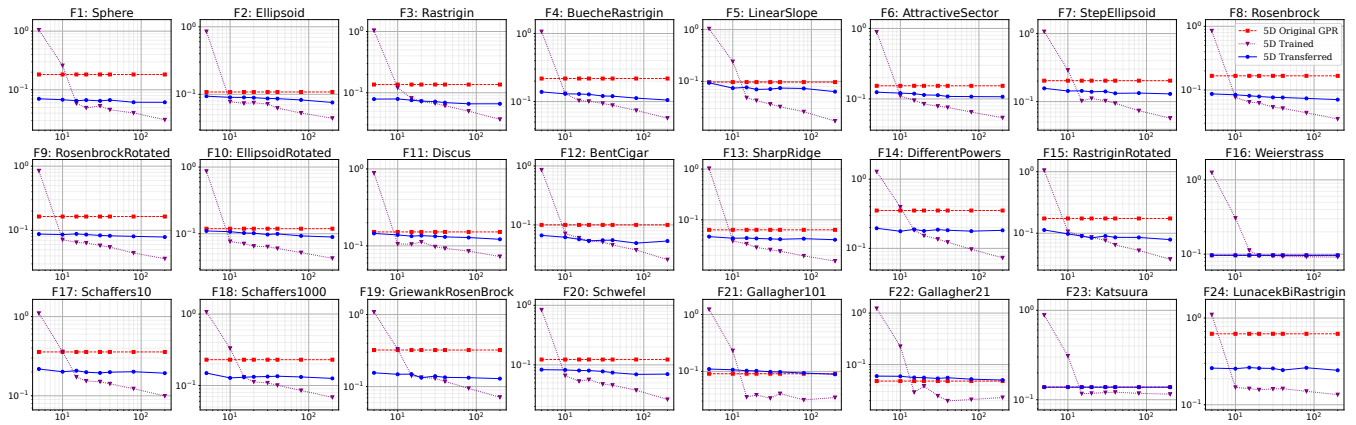


Figure 19: The SMAPE values (y -axis) for the original GPR, transferred GPR, and GPR trained solely on the transfer dataset are plotted against the transfer dataset sizes (x -axis: 5, 10, 15, 20, 30, 40, 80, 200) for 5D BBOB functions. The analysis combines a beta CDF warping function (approximating a sigmoidal transformation) with an affine transformation.

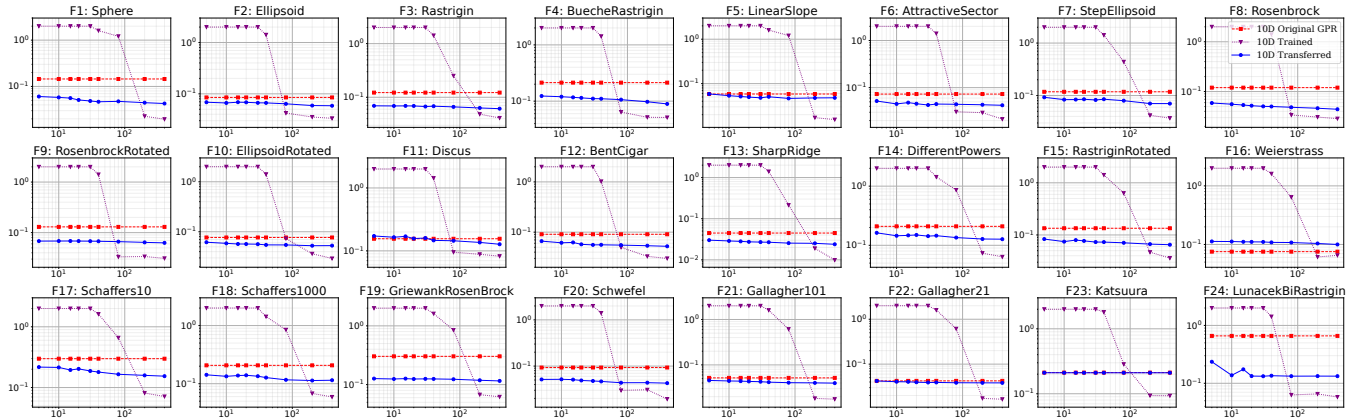


Figure 20: The SMAPE values (y -axis) for the original GPR, transferred GPR, and GPR trained solely on the transfer dataset are plotted against the transfer dataset sizes (x -axis: 5, 10, 15, 20, 30, 40, 80, 200, 400) for 10D BBOB functions. The analysis combines a beta CDF warping function (approximating a sigmoidal transformation) with an affine transformation.

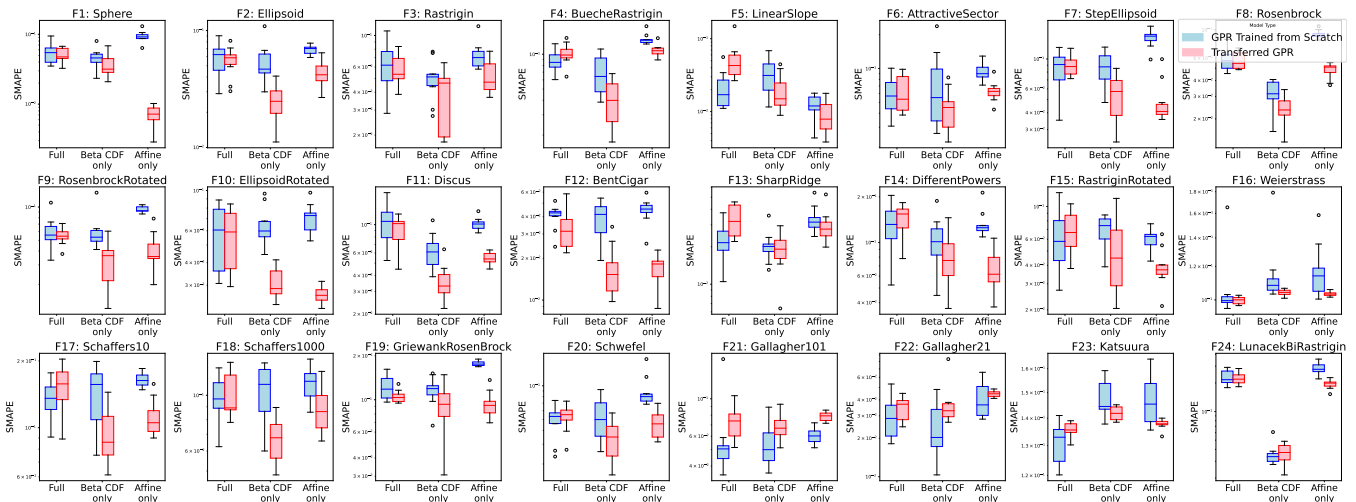


Figure 21: The ablation study focuses on the beta CDF warping function, with rotation and translation disabled, approximating an exponential transformation. We compare our results with reproduced code from [24] using box plots for 5D BBOB functions with a 20-sample transfer dataset. The plots show SMAPE values (*y*-axis) for the transferred GPR and a model trained solely on the transfer dataset across different transfer learning settings (*x*-axis).

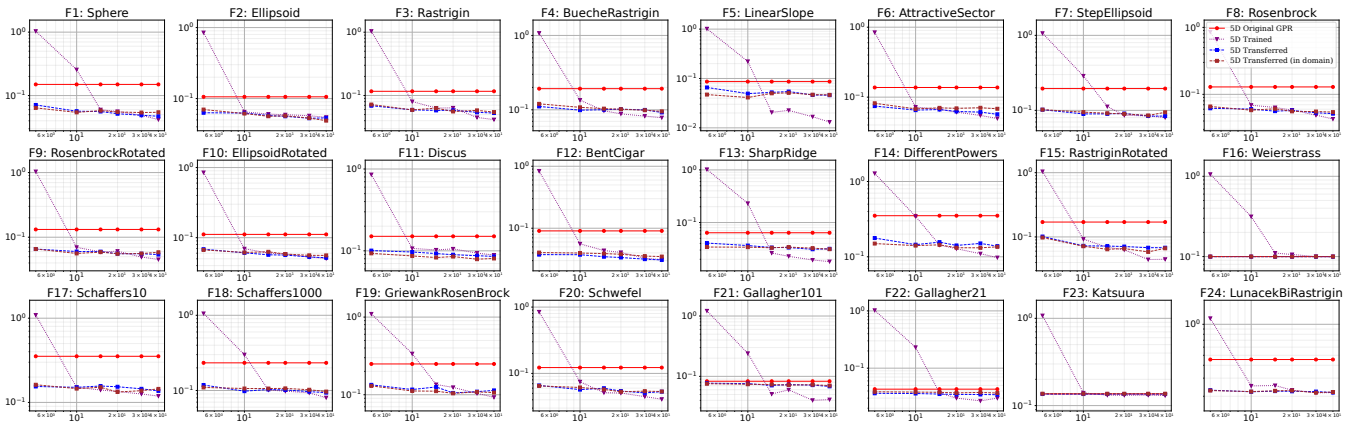


Figure 22: Ablation study presents results for the “in domain” scenario, where only transfer data—sampled from the target domain and mapped back into the original domain after transformation—is used for training. SMAPE values (*y*-axis) are shown for the original GPR, transferred GPR, and a model trained solely on the transfer dataset, plotted against transfer dataset sizes (*x*-axis: 5, 10, 15, 20, 30, 40) for 5D BBOB functions. The analysis combines a beta CDF warping function (approximating an exponential transformation) with an affine transformation.

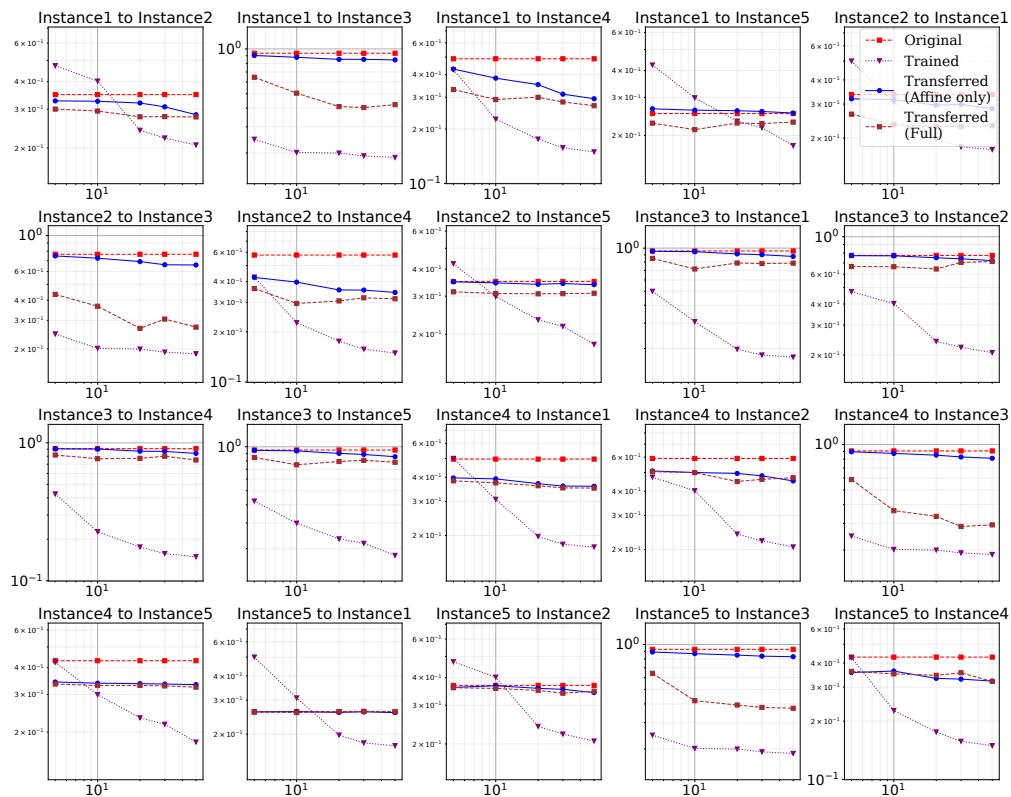


Figure 23: The study evaluates SMAPE values (y -axis) for four GPR models on an automotive industry benchmark: the original GPR model, a transferred GPR with an assumed affine transformation (“Transferred (Affine only)” [24]), a transferred GPR model using the proposed method (“Transferred (Full)”), and a model trained solely on the transfer dataset. SMAPE values are plotted against transfer dataset sizes (x -axis: 5, 10, 20, 30, and 50).